INFORMATION TO USERS

This reproduction was made from a copy of a manuscript sent to us for publication and microfilming. While the most advanced technology has been used to photograph and reproduce this manuscript, the quality of the reproduction is heavily dependent upon the quality of the material submitted. Pages in any manuscript may have indistinct print. In all cases the best available copy has been filmed.

The following explanation of techniques is provided to help clarify notations which may appear on this reproduction.

1. Manuscripts may not always be complete. When it is not possible to obtain missing pages, a note appears to indicate this.

2. When copyrighted materials are removed from the manuscript, a note appears to indicate this.

3. Oversize materials (maps, drawings, and charts) are photographed by sectioning the original, beginning at the upper left hand corner and continuing from left to right in equal sections with small overlaps. Each oversize page is also filmed as one exposure and is available, for an additional charge, as a standard 35mm slide or in black and white paper format.*

4. Most photographs reproduce acceptably on positive microfilm or microfiche but lack clarity on xerographic copies made from the microfilm. For an additional charge, all photographs are available in black and white standard 35mm slide format.*

*For more information about black and white slides or enlarged paper reproductions, please contact the Dissertations Customer Services Department.

8623724

Bosnik, James Robert, Jr.

STATIC AND VIBRATIONAL KINEMATIC PARAMETER ESTIMATION FOR CALIBRATION OF ROBOTIC MANIPULATORS

The Pennsylvania State University   Ph.D.   1986

University
Microfilms
International 300 N. Zeeb Road, Ann Arbor, MI 48106

PLEASE NOTE:

In all cases this material has been filmed in the best possible way from the available copy.
Problems encountered with this document have been identified here with a check mark __√__ .

1. Glossy photographs or pages _____

2. Colored illustrations, paper or print _____

3. Photographs with dark background _____

4. Illustrations are poor copy _____

5. Pages with black marks, not original copy _____

6. Print shows through as there is text on both sides of page _____

7. Indistinct, broken or small print on several pages __√__

8. Print exceeds margin requirements _____

9. Tightly bound copy with print lost in spine _____

10. Computer printout pages with indistinct print _____

11. Page(s) _____ lacking when material received, and not available from school or author.

12. Page(s) _____ seem to be missing in numbering only as text follows.

13. Two pages numbered _____. Text follows.

14. Curling and wrinkled pages _____

15. Dissertation contains pages with print at a slant, filmed as received _____

16. Other_____

_____

_____

University
Microfilms
International

The Pennsylvania State University

The Graduate School

**Static and Vibrational Kinematic Parameter Estimation
for Calibration of Robotic Manipulators**

A Thesis in

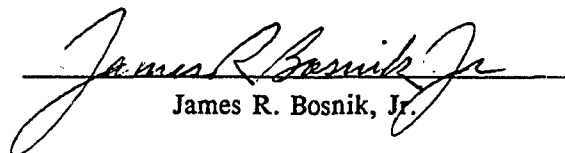Mechanical Engineering

by

James R. Bosnik, Jr.

Submitted in Partial Fulfillment
of the Requirements
for the Degree of

Doctor of Philosophy

August 1986

I grant The Pennsylvania State University the nonexclusive right to use this work
for the University's own purposes and to make single copies of the work available to
the public on a not-for-profit basis if copies are not otherwise available.

James R. Bosnik, Jr.

We approve the thesis of James R. Bosnik, Jr.

Date of Signature:

7/2/86

H. J. Sommer III, Associate Professor of Mechanical
Engineering, Thesis Advisor

30 June 86

James C. Wambold, Professor of Mechanical Engineering,
Chairman of Committee

30 June 86

Harold R. Jacobs, Professor of Mechanical Engineering,
Head of the Department of Mechanical Engineering

July 1, 1986

Vernon H. Neubert, Professor of Engineering Mechanics

July 2, 1986

William H. Park, Professor of Mechanical Engineering

6/30/86

Alok Sinha, Assistant Professor of Mechanical
Engineering

6/30/86

Martin W. Trethewey, Assistant Professor of Mechanical
Engineering

ABSTRACT

Kinematic positioning accuracy has been shown to be an important performance criterion for robotic manipulators. Estimation of the static and vibrational kinematic parameters of robotic manipulators provides means for (1) increasing the absolute static positioning accuracy of the manipulator without the expense of tighter tolerances on manipulator components, and (2) tracking the vibrational performance of the manipulator's kinematic parameters throughout its workspace with significant savings in both experimental and computational time over multiple-posture modal analysis. From experimentally obtained data, the estimation algorithms synthesize sets of "optimal" kinematic parameters using a Marquardt nonlinear least-squares optimization scheme. The optimal parameters are those which minimize error between the end effector pose predicted by a manipulator's internal kinematic model and the actual end effector pose. Both the static and vibrational algorithms have been successfully tested using data collected from a General Electric model A4 industrial robot. The most important considerations in interpreting the experimental results were found to be (1) presence of redundant parameters in the test model, and (2) estimation of the effects of input forcing direction on structural response. Both parameter estimation techniques have proven to be viable methods in the laboratory, and are being refined for practical industrial use.

TABLE OF CONTENTS

LIST OF TABLES

LIST OF FIGURES

LIST OF SYMBOLS

α_i Parameter, rotation about local z-axis, link i

β_i Parameter, rotation about local y-axis, link i

γ_i Parameter, rotation about local x-axis, link i

θ_i Joint variable, joint i

θ_{0i} Joint variable zero-reference value, joint i

σ Mean deviation of residuals (aggregate)

σ_r Mean deviation of residuals (position only)

σ_ϕ Mean deviation of residuals (attitude only)

ϕ_i General rotational displacement, estimated, dimension i

ϕ_i' General rotational displacement, measured, dimension i

a_i Parameter, translation along local x-axis, link i

b_i Parameter, translation along local y-axis, link i

c_i Parameter, translation along local z-axis, link i

$c\phi$ cosine(ϕ)

$F(s)$ Laplace transform of system input

$H(s)$ System transfer function

k_i Transducer constant, joint i

n Number of calibration postures

m Number of calibrated parameters

p_i Parameter i

r_i General translational displacement, estimated, dimension i

r_i' General translational displacement, measured, dimension i

$s\phi$ sine(ϕ)

SSQ Sum-of-the-squares of residuals (aggregate)

SSQ_r Sum-of-the-squares of residuals (position only)

SSQ_ϕ Sum-of-the-squares of residuals (attitude only)

V_i Transducer output voltage, joint i

$X(s)$ Laplace transform of system output

{ }	Braces denote vectors
[ ]	Brackets denote matrices or references, depending on context
$\{\beta\}$	Update vector
{T}	General transformation in vector form
$\{T_i\}$	Transformation in vector form, link i
[T]	General transformation in 4x4 matrix form
$[T_i]$	Transformation in 4x4 matrix form, link i
$[V_\beta]$	Update variance/covariance matrix
[X]	Jacobian matrix
{Y}	Residual vector

GLOSSARY

attitude	the rotational relationship of one coordinate frame to another
calibration point	a particular site within a particular posture
CMA	coordinate measuring apparatus
CRD	coordinate reference device
EECF	end effector coordinate frame
FFT	fast Fourier transform
FRF	frequency response function
GE A4	General Electric model A4 industrial robot/control unit
lower arm	the second-most proximal moving link of the General Electric model A4 manipulator
pose	the position and attitude of one coordinate frame relative to another
position	the translational relationship of one coordinate frame to another
posture	the unique sequential combination of a set of manipulator joint variables and physical parameters
site	a particular location within a coordinate frame (a measuring point for position and/or attitude data)
upper arm	the most proximal moving link of the General Electric model A4 manipulator

ACKNOWLEDGEMENTS

I would like to thank Professor H. J. Sommer III for his many, many contributions as Thesis Advisor. Professor Sommer's guidance, expertise, and encouragement have helped to shape this work from the outset. At the same time, and just as importantly, he has been a good friend.

Several people and organizations have provided valuable support to the research effort. I would like to thank the Department of Mechanical Engineering for providing facilities and equipment, Professor Martin W. Trethewey for his loan of the Fast Fourier Transform Analyzer, Continental Can Corporation for funding several critical pieces of research equipment, and the Engineering Computer Laboratory for use of their excellent computational facilities.

My final and most sincere thanks are to Diane Pastella for her patience and support throughout the research program. She has been at once an advisor, critic, and friend. It's her turn now.

Chapter 1

INTRODUCTION

1.1 Background

One of the fundamental interests and concerns in the design of robotic

manipulators is kinematic positioning accuracy. Accuracy, in this context, can be

defined as the maximum difference between the pose of the end of a manipulator's

arm, as calculated using the robot's internal control algorithm, and the true pose of the

end-of-arm. Generally, efforts to increase accuracy in robotic manipulators have

involved one of two approaches: (1) specification of tighter tolerances on manipulator

components and (2) calibration. The first approach requires analysis of the effects of

component tolerances on end-of-arm position, and is often accompanied by significant

increases in hardware costs to reduce mechanical compliances and laxities. The second

approach, calibration, is an alternative to the first approach and will be the focus of

the current work.

Calibration can be defined as a determination of the relationship between the

readings of measuring instruments and the true values of the quantity measured. (In

the case of robotic manipulators, the manipulator itself is the measuring instrument

with regard to positioning accuracy.) In calibration, true values of the quantity to be

measured must be obtained from accurate, external measuring systems, and

subsequently compared to the values indicated by the device being calibrated. In

general, the calibration process consists of three parts: measurement, identification,

and correction. During the measurement phase, data on the true and calculated end-

of-arm positions (and attitudes) of a manipulator is collected over its working range. In the identification phase, values for the various physical and electrical parameters of the manipulator are re-evaluated to find "optimal" parameter values which produce the least error between calculated and true positions at each calibration posture. Lastly, in the correction phase, actual modifications are made to the manipulator's control algorithm and/or hardware to effect the desired increases in accuracy. Another important use of the optimal parameters is their inclusion in a time-history database for tracking potential component damage in a manipulator predictive maintenance program.

Calibration of robotic manipulators may be carried to various degrees of sophistication and complexity. Specifically, calibration may be: (1) static, (2) vibrational, or (3) dynamic. For static calibration, the manipulator is held in various postures while data on the true and calculated absolute end-of-arm poses is collected. Vibrational calibration adds the effects of small structural oscillations about the static equilibrium postures to the static calibration procedure. Ultimately, dynamic calibration adds the effects of gross manipulator motion to the static and vibrational calibration procedures. The first two levels of calibration, static and vibrational, are explored in this work.

The following definitions will be used throughout this work:

- position: the translational relationship of one coordinate frame to another

- attitude: the rotational relationship of one coordinate frame to another

- pose: the position and attitude of one coordinate frame relative to another

- site: a particular location within a coordinate frame (a measuring point for position and/or attitude data)

- posture: the unique sequential combination of a set of manipulator joint variables and physical parameters

- calibration point: a particular site within a particular posture

1.2 Problem Statement

The primary objectives of this study were the development and testing of an algorithm which will enable one to carry out the calibration of a robotic manipulator. Specifically, meeting these objectives involved:

1. design of an algorithm to carry out the static calibration of a robotic manipulator,

2. numerical implementation of the static calibration algorithm,

3. testing of the static calibration algorithm via numerical simulation of various robots,

4. testing of the static calibration algorithm using data from a real industrial robot,

5. modification and extension of the static calibration algorithm to carry out the vibrational calibration of a robotic manipulator,

6. numerical implementation of the vibrational calibration algorithm, and

7. testing of the vibrational calibration algorithm using data from a real industrial robot.

The scope of the study was limited to static and vibrational calibration of robotic manipulators. Future studies may include dynamic calibration, a natural extension of the present work.

Chapter 2

STATIC CALIBRATION

2.1 Introduction

Several investigators have shown that accuracy is an important performance criterion for robotic manipulators. Kinzel and Hall [1] showed that position errors in spatial linkages can be significant and proposed means of predicting and verifying their accuracy. Mooring [2] found that very small errors in joint alignment could cause significant errors in end effector positioning, and that absolute positioning accuracy for a typical industrial robot may be as much as 1.25 inches. Mooring also discussed the advantages of using a calibration approach to increase manipulator accuracy over trying to build a "perfectly aligned robot." More recently, Stauffer [3] and Colson and Perriera [4] have stated the importance of accuracy as a manipulator performance criterion, especially in light of the ever-increasing interest in offline programming of industrial robots.

The accuracy of a robotic manipulator is dependent on the accurate knowledge of the kinematic and electrical parameters which describe the manipulator's mechanical linkage and incorporated transducers. Because certain linkage parameters may not initially be estimated with a high degree of confidence due to component compliance, assembly errors, or difficult gauging, numerical re-evaluation of these parameters in a calibration scheme will provide a better analytical description of the robotic manipulator and produce superior manipulator accuracy.

Such a calibration scheme may be formulated as a dimensional synthesis of manipulator parameters based on data taken from mechanical measurements [5]. The functional inputs (manipulator joint transducer signals) must be recorded simultaneously with the desired functional outputs (actual manipulator calibration positions and attitudes). An iterative numerical optimization routine may then be used to adjust manipulator parameters so as to minimize manipulator end effector coordinate frame (EECF) error over the selected calibration range (usually the entire workspace of the manipulator).

From a kinematic standpoint, this calibration may be expressed as a multiple-point synthesis of a spatial open-loop mechanism for rigid-body guidance. Similar syntheses of closed-loop spatial linkages by Tull and Lewis [6] and Chen and Chan [7] have been successfully performed using variations of the Marquardt nonlinear least-squares optimization algorithm [8]. Extension of these methods to open-loop synthesis is straightforward in that no loop closure constraints need be included in the input/output expressions. More recently, an algorithm was developed by Sommer and Miller [5] for the calibration of instrumented spatial linkages. This algorithm may be extended and applied to the calibration of robotic manipulators.

Several varying approaches to static calibration of robotic manipulators have been proposed. Scheffer [9] outlined the static calibration process as an iterative, nonlinear optimization, but did not provide analytical development of the method or results of experimental work. In addition to characterizing typical robot accuracy, Mooring [2] proposed a scheme to calibrate the effects of manipulator joint misalignment. Spur, Duelen, and Kirchoff [10] proposed a calibration method similar to Scheffer's [9], but with a detailed development of the mathematical approach and limited numerical simulation results. In an extension of Mooring [2], Mooring and Tang [11] discussed improvements in the external pose-measurement system required for manipulator calibration. In this work, the authors also allowed for measurement of end effector pose data at a number of postures greater than the minimum number required, to effectively decrease the influence of measurement errors. None of the above

investigations [9-11], however, provided results from experimental investigations of real robots. Whitney, Lozinski, and Rourke [12] were the first to publish an investigation of robot calibration which included actual experimental results. Their approach was unique in that it included the effects of non-geometric errors, such as joint compliance, gear transmission error, and backlash, in the calibration process. Kirchner, Gurumoorthy, and Prinz [13] have recently proposed calibrating robots via a parameter perturbation approach which avoids the problem of redundancy in the parameter set. These authors outlined an approach to deal with this redundancy through careful selection of the calibration postures. Ibarra and Perreira [14] propose a calibration method similar in many ways to Scheffer [9], Spur, Duelen, and Kirchoff [10], and Whitney, Lozinski, and Rourke [12], but with particular attention given to (1) solution of the inverse kinematic problem when the Jacobian matrix is singular, and (2) using the minimum possible set of pose-measurement data. Hsu and Everett [15] also concentrated on easing the process of data collection, and proposed a method similar to Mooring and Tang [11], using permanent pose reference points within the manipulator's workspace. Most recently, Stone, Sanderson, and Neuman [16] have presented a calibration method which utilized a different kinematic model from previous works. These investigators are the only ones, aside from Whitney, Lozinski, and Rourke [12], to present experimental results. In these results, the authors find "dramatic" differences between optimized parameters and the corresponding physical manipulator parameters.

The calibration method proposed herein incorporates some of the most desirable features of the above schemes with some new features, and represents a general, flexible, efficient method for the static calibration of robotic manipulators. Specifically, features combined or added include:

- use of multiple (many) postures (combined)

- allowance for nonlinear transducers (combined)

- allowance for extended parameter sets (added)

- use of Marquardt nonlinear solution algorithm, providing more robust convergence (added)

- allowance for multiple calibration sites per calibration posture (added)

- options for position and/or attitude data collection (added)

- options for use of exact or estimated partial derivatives, allowing manipulator/ algorithm independence (added)

- allowance for analysis of variance of updates (added)

Each of the features above will be expanded upon in the sections which follow.

From a practical standpoint, the body of parameter data generated by a static calibration will be very useful in identifying and isolating points of damage or wear before such problems might become discernible by other means. If a static calibration is performed on a particular robotic manipulator at regular time intervals (every month, for instance), then the values of the various parameters can be compared to their corresponding values during previous tests, for the purpose of identifying those parameters whose values are changing more than an acceptable or expected amount. After additional experience with the static calibration procedure, it may be possible to make specific maintenance or repair recommendations for a manipulator on the basis of its static calibration history.

2.2 Kinematic Modeling

The most general robotic manipulator is an open-loop six-degree-of-freedom kinematic chain composed of a base and an end effector connected by five intermediate links and six intermediate joints, as shown in Figure 2.1. Knowledge of the joint variables and the physical dimensions of the intermediate links allows description of the relative spatial position and attitude of one end link relative to the other. Although this particular work deals with a six-degree-of-freedom manipulator having revolute or prismatic joints, the calibration technique described below may

ELBOW EXTENSION

SHOULDER SWIVEL

YAW

ROLL

ARM SWEEP

PITCH
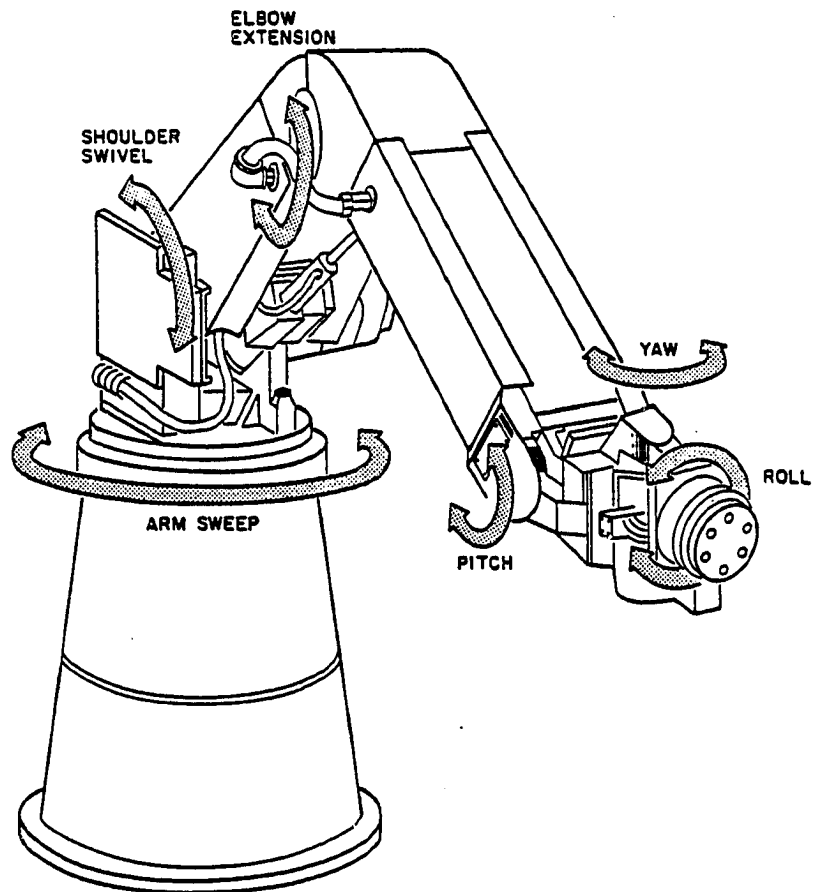
Figure 2.1: General Six-Degree-of-Freedom Robotic Manipulator

easily be adapted to other manipulators with differing types of joints and numbers of degrees-of-freedom.

Kinematically, relative spatial position and attitude may be described by a matrix transformation from a coordinate frame located on the base (fixed frame) to an EECF (moving frame), or

$$\{1 \ x \ y \ z\}^T_{fixed} = [T] \ \{1 \ x \ y \ z\}^T_{moving} \ .$$ (2.1)

This transformation may be formed by the product of six link transformation matrices which describe the separation, orientation, and joint movement of succesive joint axes, as follows:

$$[T] = [T_1][T_2][T_3][T_4][T_5][T_6] \ .$$ (2.2)

These matrices are standard kinematic notation for describing coordinate transformations from the fixed coordinate frame to the moving frame along a chain of coordinate frames located on intermediate links [17]. Other kinematic methods which utilize separate link shape matrices and pair variables [18] may also be used. Appendix A provides a summary of both of the kinematic models described above.

The fundamental task of a robotic manipulator is to deliver its end effector to a known position and attitude relative to a fixed, pre-defined coordinate frame. This relationship between the moving (end effector) coordinate frame and the fixed (base) coordinate frame may be expressed by a coordinate transformation as above. More succinctly, the relationship may be expressed by a radial vector from the origin of the fixed frame to the origin of the moving frame and an ordered set of three Euler angles describing the relative attitude of the two frames. The three radial vector components r_i and the three ZYX-ordered Euler angles ϕ_i as components of the transformation matrix [T] may be expressed as

$$[T] = \begin{bmatrix} 1 & 0 & 0 & 0 \\ r_1 & c\phi_1 c\phi_2 & c\phi_1 s\phi_2 s\phi_3 - s\phi_1 c\phi_3 & c\phi_1 s\phi_2 c\phi_3 + s\phi_1 s\phi_3 \\ r_2 & s\phi_1 c\phi_2 & s\phi_1 s\phi_2 s\phi_3 + c\phi_1 c\phi_3 & s\phi_1 s\phi_2 c\phi_3 - c\phi_1 s\phi_3 \\ r_3 & -s\phi_2 & c\phi_2 s\phi_3 & c\phi_2 c\phi_3 \end{bmatrix}, \qquad (2.3)$$

where $s\phi$=sine(ϕ) and $c\phi$=cosine(ϕ).

The consecutive link/joint transformations $[T_i]$ above may be described most fundamentally by three link parameters and a single joint variable [17]. Therefore, a minimum of 21 manipulator link parameters and six kinematic pair variables must be defined or measured to calculate the overall manipulator transformation. This simple set of link parameters, however, does not allow the designer to arbitrarily assign intermediate coordinate frame locations along the linkage chain when formulating the individual link kinematic transformations [5]. These basic link parameters require specific definition of coordinate frame axes orientations and origin locations according to established kinematic conventions [17]. These 21 kinematic parameters remain constant during a particular experimental session and must be determined exactly to produce accurate manipulator performance.

Although a minimum of 21 kinematic parameters is necessary to calculate the overall manipulator transformation, other choices are possible and may be advantageous [18]. Link parameter sets with more than the minimum number of parameters may be chosen to be equivalent to the minimum set. Choice of a kinematic parameter set with more than 21 parameters will add a small amount of computational time to the calibration process to estimate these redundant paramters, but also may simplify the analyst's job considerably.

The six joint variables must be measured accurately during the course of the experimental session. For the revolute or prismatic joints commonly found in robotic

manipulators, transducers in common use include potentiometers, synchros, resolvers, contact encoders, and non-contact magnetic or optical encoders. Assuming linearized transducer performance over the calibration space, two electrical parameters per joint (transducer output slope k_i and zero point offset θ_{0i}) are required to transform an experimentally measured transducer output voltage (or digital count) V_i into the corresponding revolute pair variable value θ_i, as shown in Equation 2.4.

$$\theta_i = k_i V_i + \theta_{0i} \tag{2.4}$$

Assuming accurate definition of the 21 physical link parameters and the 12 electrical joint transducer parameters described above, the radial vector components and Euler angles at any instantaneous manipulator posture will be a vector function of the six measured joint transducer voltages and the parameter estimates p_i as shown in Equation 2.5.

$$\{r_1, r_2, r_3, \phi_1, \phi_2, \phi_3\}^T = f(V_1, V_2, V_3, V_4, V_5, V_6, p_1, p_2, p_3, ..., p_{33}) \tag{2.5}$$

Again, 33 parameter estimates (21 physical and 12 electrical) are the minimum required; choice of an expanded kinematic parameter set may increase this number. A block diagram of the manipulator kinematic model changing joint transducer voltages into a spatial position and attitude description is shown in Figure 2.2.

There are several areas where errors affecting static manipulator accuracy may appear in this model. The most suspect areas are in the determination of the physical and electrical parameters. Mechanical components may be accurately machined, gauged, and assembled in the laboratory; however, link flexure or permanent deformation, joint compliance, and manipulator assembly/modification may make exact knowledge of certain individual parameter values nearly impossible. It is a purpose of this work to describe a method for the iterative numerical estimation of such
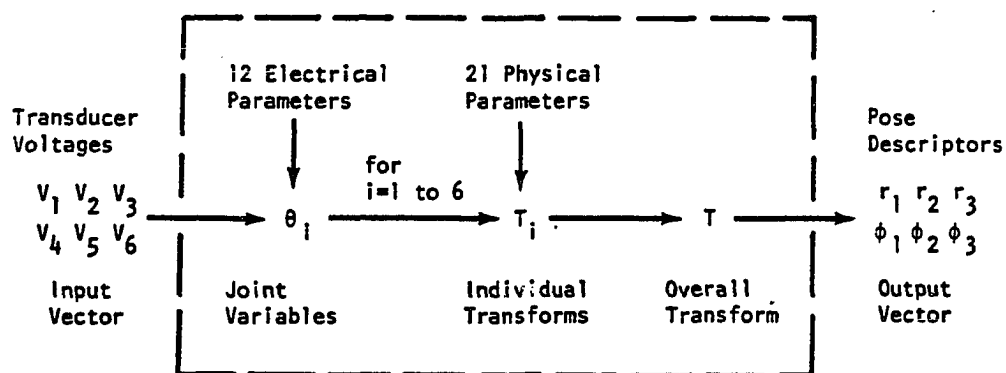
Figure 2.2: Block Diagram of the Manipulator Kinematic Model (after Sommer and Miller [5])

parameters based on a carefully performed static mechanical calibration of the fully assembled robotic manipulator.

2.3 Calibration

2.3.1 Measurement

The mechanical calibration should place the moving and fixed ends of the manipulator in several exactly known relative positions and attitudes and measure the corresponding transducer output voltages at these postures. The accuracy of the manipulator at each posture may then be defined as the difference between the measured relative pose quantities (radial vector components and Euler angles) and the expected pose quantities (as determined using the manipulator kinemetic model). Accumulation of this accuracy measurement at many such postures over the anticipated range of manipulator motion will allow re-evaluation of initial estimates of the physical and electrical parameters to minimize the aggregate error over the calibration space.

Mechanical measurement of the relative attitude terms in Euler-angle form may be infeasible or undesireable. An alternative in this case is to measure the positions of three (or more) non-collinear sites on the manipulator's end effector. This multiple-point position data may then be either converted immediately to Euler-angle form or input directly to the calibration algorithm in the form of additional calibration points. This concept may be extended to apply to intermediate manipulator links, allowing a general choice of multiple calibration sites (on several links) per manipulator calibration posture.

External measurement of manipulator pose data may be accomplished by any of several means, including instrumented milling tables and dividing heads, gauge blocks [5], physically contacting coordinate verifiers [19], and non-contacting sonic transducers [20], laser transducers [21,22], or coordinate verifiers [23]. Regardless of which method is chosen, three basic considerations must be satistifed: (1) positoning precision and knowledge of the relative position and attitude at each calibration posture must be

significantly better than the desired manipulator accuracy, (2) measurement of the transducer output signals must be at least as accurate as desired manipulator accuracy, and (3) a sufficient number of calibration postures should be measured so as to representatively populate and span the desired manipulator workspace. The number of calibration postures should be greater than one-sixth the number of estimated parameters (if using all six pose quantities at each calibration posture, that is, three radial vector components and three Euler angles).

2.3.2 Identification

The identification portion of this calibration scheme may be formulated as a nonlinear optimization of the manipulator's physical and electrical parameters, similar to kinematic dimensional synthesis of mechanisms for multiple input/output function generation [5,7]. The measured joint transducer voltages at each calibration posture may be viewed as the function generator input vector. The radial vector components and Euler angles calculated by the manipulator kinematic model (based on parameter estimates and the input vector) may be viewed as the estimated function generator output vector. The exactly known radial vector components and Euler angles at each mechanical calibration posture may be viewed as the desired function generator output vector. The manipulator's electrical parameters may be viewed as scaling factors, converting the voltage inputs into a set of angular inputs to the mechanism. The manipulator's physical parameters correspond to the mechanism link dimensions.

The optimization process must then synthesize a set of the manipulator's physical and electrical parameter estimates which produce the best possible function generation as described by an aggregate measure of the difference in desired and calculated output vectors over all calibration points. This process may be done iteratively by evaluating the aggregate function generation error for an estimated parameter set, and, based on various gradient and search techniques, minimizing that aggregate error through simultaneous modifications of the several parameter estimates.

If certain of the manipulator's physical or electrical parameter values may be considered well-defined (for instance, well-gauged dimensions of rigid links), such parameters need not be optimized. This allows significant computational reduction while not placing any further restrictions on the other parameters. As described by Sommer and Miller [5], only three restrictions on the parameter set must be enforced when using the Denavit-Hartenberg link formulation [17]: (1) if any physical parameter estimates are modified, all six joint transducer zero-point parameters must also be simultaneously modified to account for joint transducer zero-shift, (2) all three physical parameter estimates for a single link must be simultaneously modified to allow intermediate coordinate frame rearrangement, and (3) a fourth physical parameter must be added to accurately describe the last link in a chain of parameter-modified links for final coordinate frame alignment.

In addition, kinematic models which include redundant parameters may be used, depending on the robustness of the optimization algorithm. The redundant parameters may not preclude an optimal solution but will tend to numerically wander even at solution convergence. The kinematic model described above provides the basis for the minimum manipulator parameter set required for efficient simultaneous parameter optimization.

In order to search for improved manipulator parameter estimates which produce superior accuracy over the entire calibration space, a rigorous definition of aggregate accuracy must be chosen. The definition used in this work is the classical sum-of-the-squares error criterion as shown in Equations 2.6, 2.7, and 2.8.

$$SSQ_r = \sum_{i=1}^{n} [(r_1'-r_1)^2 + (r_2'-r_2)^2 + (r_3'-r_3)^2] \qquad (2.6)$$

$$SSQ_\phi = \sum_{i=1}^{n} [(\phi_1'-\phi_1)^2 + (\phi_2'-\phi_2)^2 + (\phi_3'-\phi_3)^2] \qquad (2.7)$$

$$SSQ = SSQ_r + SSQ_\phi \tag{2.8}$$

This formulation accumulates the squares of the three position residuals and the squares of the three attitude residuals at each calibration point. The primed terms above are known position and attitude values determined by the mechanical calibration hardware and the unprimed terms are position and attitude values calculated using an estimated manipulator kinematic model at n calibration postures. (This formulation may differ slightly for cases in which multiple calibration sites per calibration posture are used or in which angular data is not measured.) Minimizing the sum-of-the-squares of the position and attitude residuals leads [8] to solution of the matrix equation

$$\{\beta\} = ([X]^T[X])^{-1} ([X]^T\{Y\}) \quad , \tag{2.9}$$

where $\{\beta\}$ is the vector of parameter updates, $[X]$ is the system Jacobian matrix, and $\{Y\}$ is the vector of pose residuals. Once the update vector $\{\beta\}$ is obtained, it is added to the vector of current parameter values, and the process continues iteratively until such time that a pre-defined stop criterion is met.

When using any sum-of-the-squares criterion, weighting techniques may be used to reduce (or accentuate) the effects of various residuals. For example, if a particular calibration posture consistently demonstrates poor mechanical calibration precision, the residuals at this posture may be numerically weighted less heavily than residuals at other postures in the grand sum accumulation. Also, relative weighting between position and attitude residuals at each calibration site may be used to synthesize a manipulator parameter set which tends to predict position measurements more accurately than attitude measurements or vice versa.

The optimization technique chosen to minimize the above sum-of-the-squares for the numerical calibration is a nonlinear unconstrained regression algorithm as formulated by Marquardt [8]. This method is a mixture of Taylor series (or Gauss-Newton) methods and simple gradient search techniques. For parameter estimates far

from optimum, gradient techniques prevail, while Taylor series techniques, which require better estimates, are stronger near the optimum.

2.3.3 Correction

Correction, in the case of static calibration, typically consists of modifying the control algorithm (also known as the mathematical model or the geometrical model) of the manipulator in question. As it relates to static calibration, the control algorithm must meet two contradictory requirements [9]:

1. the control algorithm must operate correctly given the accuracy of the static calibration algorithm (as discussed in Section 2.3.1), and

2. speed of execution of the control algorithm should be rapid enough so that the manipulator's performance is not degraded (the more complicated the algorithm, the slower the execution).

During correction, parameter values from the identification phase of the calibration are inserted as constants into their respective places in the control algorithm. This process typically consists of modifying specific controller memory locations which hold values representing physical manipulator parameters. Immediately following correction, static accuracy of the manipulator under calibration will be within the limits imposed by the control algorithm, by manipulator hardware, or by the calibration algorithm itself.

2.3.4 Numerical Simulation

After development of the static calibration algorithm and implementation in VAX FORTRAN on a VAX 11/785 minicomputer, several numerical simulations were undertaken to verify correct operation of the coded algorithm. All phases of the simulation were performed using mathematical models of two real robots, the International Robomation/Intelligence (IRI) manipulator and an IBM model RS-1 manipulator. Phases of the simulation were the following:

1. Forward kinematic solutions were performed for 30 representative postures sufficient to populate and span the manipulator workspace. These solutions represented a set of equivalent joint variables/end effector pose data for a geometrically perfect manipulator.

2. Inverse kinematic solutions were performed for each of the postures of Step 1, using Step 1 results for input. This step verified that the inverse kinematic (closure) algorithm was working properly, and also that the results of Step 1 were correct.

3. Forward kinematic solutions were performed for the 30 representative postures of Step 1 using perturbed values of the joint variables. These solutions represented a set of equivalent joint variables/end effector pose data for an imperfect manipulator.

4. Inverse kinematic solutions were performed for each of the postures of Step 3, again verifying the inverse kinematic (closure) algorithm and also the Step 3 results.

5. Static calibrations were performed, using or referencing data for the 30 representative postures from each of the above steps. In all simulation cases, the static calibration algorithm proved to be predictable, efficient, and robust.

After the complete calibration algorithm was verified, several other aspects of its operation were tested, as described below.

The Marquardt algorithm described above requires a complete set of first partial derivatives of the residual functions with respect to the estimated parameters. Separate trials using numerical (estimated) and analytical (exact) partial derivatives were both successful. While analytical partial derivatives are more accurate and efficient (with regard to the closure process), they have the disadvantage of being manipulator-specific; that is, they change with the nature of the individual parameters under consideration. This factor may cause the requirement of coding modification if the

same calibration program is to be applied to different robotic manipulators or manipulator configurations. On the other hand, numerical partial derivatives apply equally well to any type of variable manipulator parameter, and thus would be more desirable from a practical standpoint, provided that their use did not prevent closure or make the closure process significantly more time-consuming.

Both analytical and numerical partial derivatives have been tested in the closure process with the following results:

1. Convergence using numerical partial derivatives was successful in all cases where convergence using analytical partial derivatives was successful.

2. Increases in computational time for convergence using numerical partial derivatives over convergence using analytical partial derivatives ranged from 0 to 25%.

Noise in the voltage or position data can adversely affect the convergence properties of any iterative, nonlinear solution algorithm. Several test cases were run in which noise was introduced into the voltage and position input data in amounts randomly distributed between ±20% of the nominal voltage and position values. Convergence was found to be unaffected by even these conservatively large noise levels.

The transformation relating kinematic data in one coordinate system to that in another may take any of several forms, as discussed in Section 2.2. Choice of a different particular form for this transformation data should not affect the ultimate convergence of the closure process; however, the closure process itself will be altered, since the form of the transformation data has an important effect on the system Jacobian matrix. There may, in a particular calibration situation, be advantages to choosing one form of the transformation data over another, including ease of data collection, entry, and interpretation.

Two forms of the transformation data were tested for their affects on the closure process and convergence. These forms were (1) the full 4 x 4 transformation matrix, as described in Equation 2.3, and (2) the equivalent transformation data in the form of three orthogonal translations and three Euler angles, which may be expressed as

$$
\{T\} = \begin{Bmatrix} r_1 \\ r_2 \\ r_3 \\ \phi_1 \\ \phi_2 \\ \phi_3 \end{Bmatrix} . \tag{2.10}
$$

The calibration algorithm performed well using both of the above descriptions; the second form, described by Equation 2.10, was used throughout most of the experimental calibration runs for its ease of data interpretation. When transformation data in the form of Equation 2.10 is used, the system Jacobian matrix *for a single posture* takes on the expanded form

$$
[X] = \begin{bmatrix}
\dfrac{\partial r_1}{\partial p_1} & \dfrac{\partial r_1}{\partial p_2} & \dfrac{\partial r_1}{\partial p_3} & \cdots & \dfrac{\partial r_1}{\partial p_m} \\[2ex]
\dfrac{\partial r_2}{\partial p_1} & \dfrac{\partial r_2}{\partial p_2} & \dfrac{\partial r_2}{\partial p_3} & \cdots & \dfrac{\partial r_2}{\partial p_m} \\[2ex]
\dfrac{\partial r_3}{\partial p_1} & \dfrac{\partial r_3}{\partial p_2} & \dfrac{\partial r_3}{\partial p_3} & \cdots & \dfrac{\partial r_3}{\partial p_m} \\[2ex]
\dfrac{\partial \phi_1}{\partial p_1} & \dfrac{\partial \phi_1}{\partial p_2} & \dfrac{\partial \phi_1}{\partial p_3} & \cdots & \dfrac{\partial \phi_1}{\partial p_m} \\[2ex]
\dfrac{\partial \phi_2}{\partial p_1} & \dfrac{\partial \phi_2}{\partial p_2} & \dfrac{\partial \phi_2}{\partial p_3} & \cdots & \dfrac{\partial \phi_2}{\partial p_m} \\[2ex]
\dfrac{\partial \phi_3}{\partial p_1} & \dfrac{\partial \phi_3}{\partial p_2} & \dfrac{\partial \phi_3}{\partial p_3} & \cdots & \dfrac{\partial \phi_3}{\partial p_m}
\end{bmatrix} . \tag{2.11}
$$

2.3.5 Experimental Investigation

2.3.5.1 Apparatus

The static parameter estimation algorithm was tested on a General Electric model A4 (GE A4) industrial robot. The test set-up consisted of four major parts: the robot itself, the robot control unit, the coordinate-measuring apparatus (CMA), and the instrumentation.

The industrial robot used in testing was the four-degree-of-freedom, electrically actuated GE A4 manipulator, designed primarily for assembly tasks (a typical SCARA-class manipulator). A schematic drawing of the GE A4 manipulator showing coordinate systems used in defining the manipulator kinematic model is shown in Figure 2.3. Joints one, two, and four (beginning at the proximal end) are each revolute with their axes of revolution running vertically. Joint three is a prismatic joint with its axis also running vertically. All joints are actuated by DC servomotors which drive harmonic gear reducers which, in turn, drive the appropriate joint, either directly or through a linkage or chain coupling. As specified by the manufacturer, maximum manipulator payload was 4.4 pounds, including the end effector, and repeatability was 0.002 inches. Figure 2.4 shows the workspace of the GE A4. As configured, the GE A4 was programmable only in a teach/playback mode; that is, offline programming was not possible. (Throughout this work, "upper arm" will refer to the most proximal moving link, and "lower arm" to the second-most proximal moving link of the General Electric model A4 manipulator.)

The GE A4 robot control unit consists of the power supplies, microcomputer hardware and software, control panel, display, teaching pendant, and other elements necessary for proper operation of the GE A4 manipulator. The control unit is connected to the manipulator through a series of multiple-conductor cables, and receives electrical power from an external 120-volt, 60-Hertz supply.

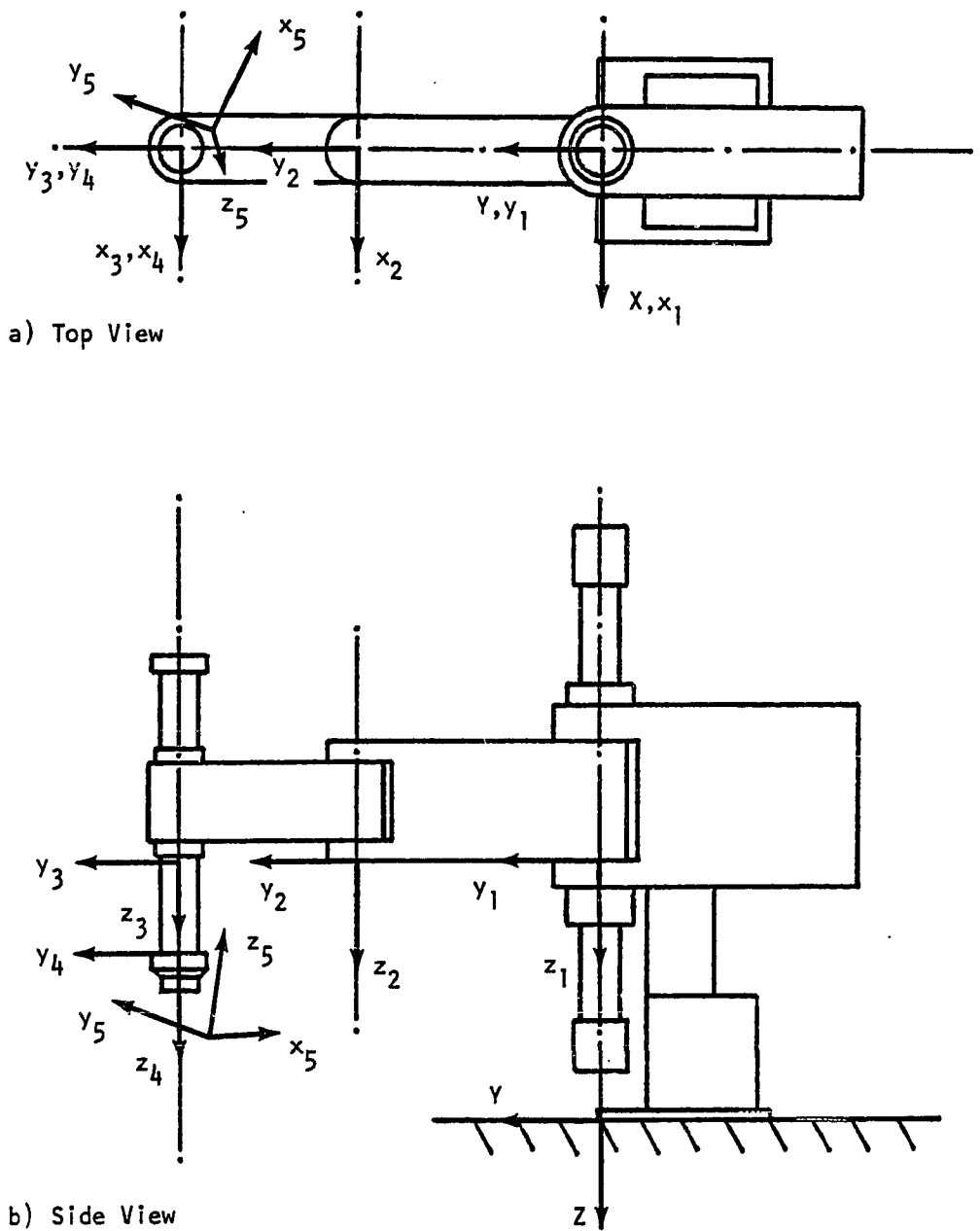Figure 2.3: Schematic of the General Electric Model A4 Manipulator

11.81"

2.5°

152.5°

200° 30°

7.13"

27.56"

15.75" 152.5°

11.81"

a) top view

2.5°
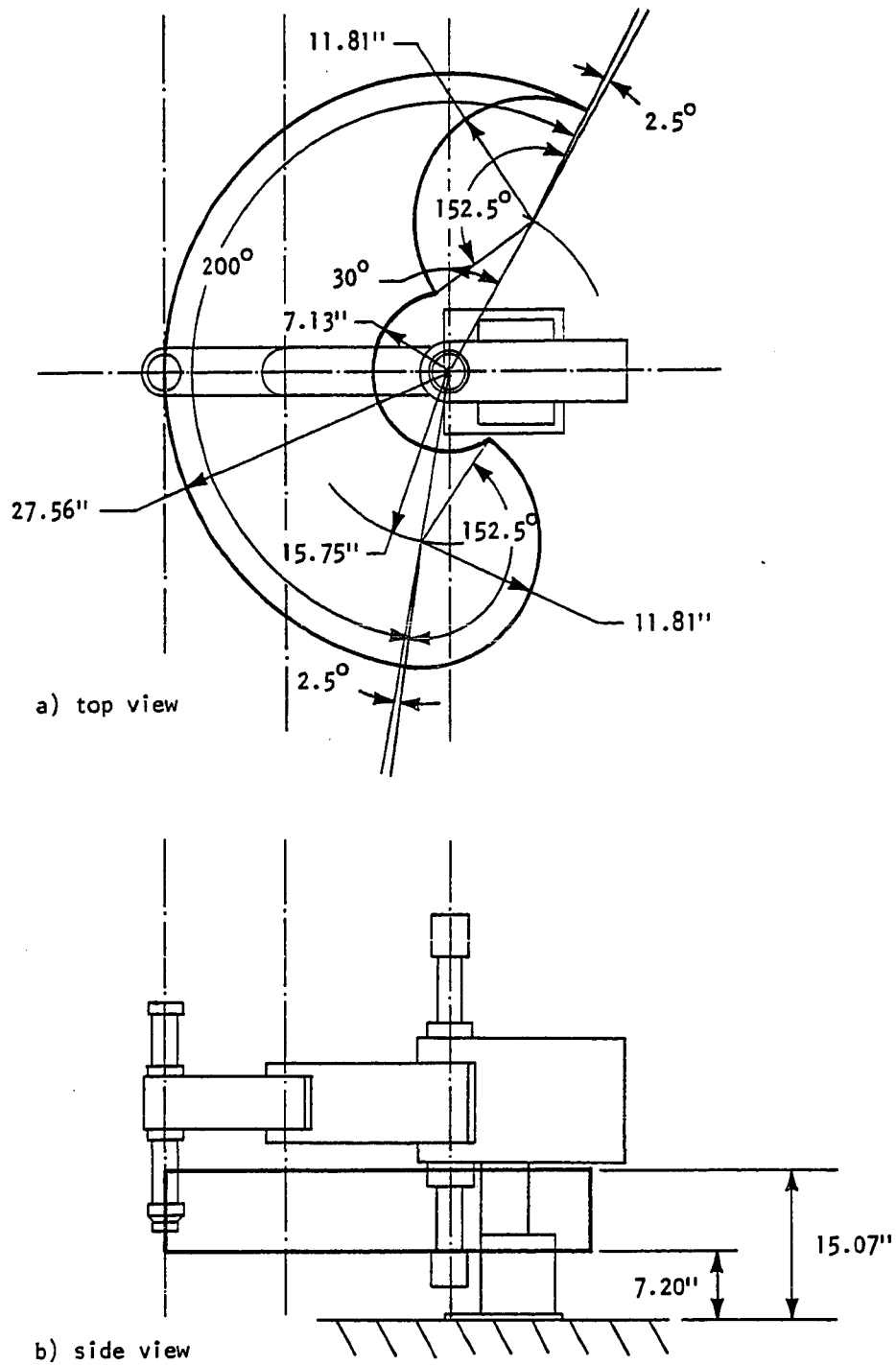
15.07"

7.20"

b) side view

Figure 2.4: Workspace of the General Electric Model A4 Manipulator

The coordinate-measuring apparatus (CMA) was designed and built specifically for this investigation, and is shown schematically in Figure 2.5. It consists of three linear, orthogonal axes arranged such that each can be moved independently of the others. A 1/4-inch by 1/2-inch by 4-inch aluminum bar was attached to the moving portion of the z-axis for the purpose of contacting the coordinate reference device squarely in any of the three coordinate directions.

A coordinate reference device (CRD) was designed and constructed to provide reference points for external pose measurement by the CMA during data collection. A schematic drawing of the CRD is shown in Figure 2.6. The CRD consisted of three 1/2-inch metal balls which were attached by three thin metal rods to a circular base. The metal balls served as contact points for the aluminum contact bar of the CMA. Three balls were used so that both position and attitude could be calibrated while measuring only positional data, as described in Section 2.3.1. The CRD was attached to the manipulator arm in the normal end effector position.

A simple electronic instrumentation circuit was utilized to indicate, with a high degree of precision, contact between the balls of the CRD and the aluminum bar of the CMA. Observation of a contact current flux was used as a definition of contact between the CRD and the CMA.

2.3.5.2 Procedure

Before actual calibration data was collected, several preliminary data collection runs were made to check performance of the robot and the CMA. These preliminary runs provided data for the testing of (1) CMA repeatability (precision), (2) effects of warm-up on manipulator performance, and (3) GE A4 repeatability.

As stated in Section 2.3.1, positioning precision and knowledge of the relative position and attitude at each calibration posture must be significantly better than desired manipulator accuracy. To test precision of the CMA, a fixed position of the
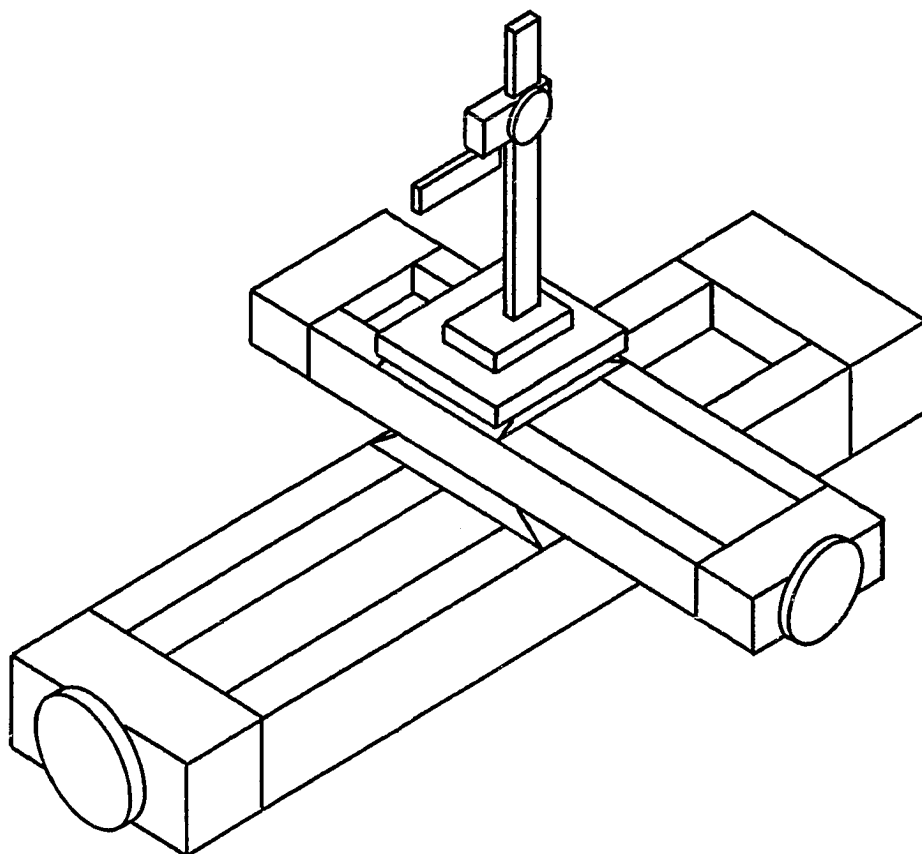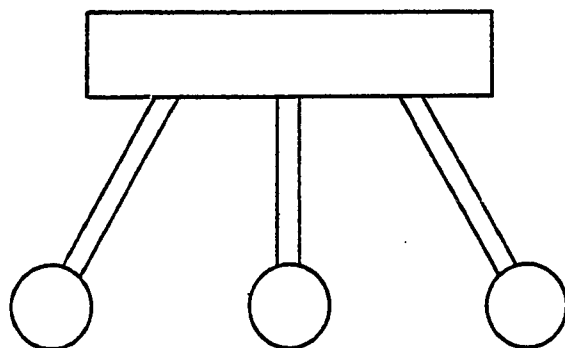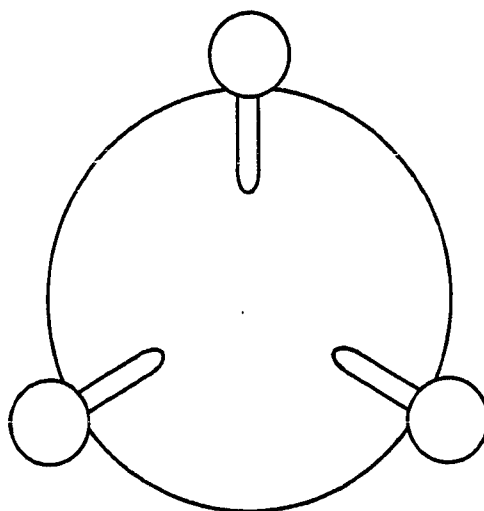
Figure 2.5: Schematic of the Coordinate Measuring Apparatus

a) side view

b) bottom view

Figure 2.6: Schematic of the Coordinate Reference Device

end effector was measured repeatedly. This process was repeated for other postures (other fixed end effector positions) throughout the manipulator's workspace.

Warm-up of various manipulator system components has been shown to have a significant effect on end effector positioning accuracy [24,25]. To test for these effects in the GE A4, an initial run was made in which the manipulator was zeroed cold, and then commanded to a pre-taught reference position, at which end effector position was measured. After a short time interval, the manipulator was cycled off and on, re-zeroed, and commanded to the same reference postion, where the end effector position was again measured. This process was repeated over several hours time.

The third preliminary data collection run was made to test manipulator repeatability. Knowledge of the GE A4's repeatability was necessary both to confirm manufacturer's specifications and to separate the effects of manipulator repeatability form manipulator accuracy. To test repeatability, the GE A4 was commanded to a pre-taught reference position, where end effector position was measured. Then, the GE A4 was moved, at random, to another posture. From this posture, the manipulator was commanded to the same reference positon as above, where end effector position was again measured. This process was repeated many times at each of several postures throughout the manipulator's workspace.

After the preliminary data collection runs were completed, four runs were undertaken to provide data for calibration of the GE A4 and to further test the calibration algorithm itself. Data collection for each of the calibration runs proceded in the same general manner, as follows. In the first experimental posture of a run, the CMA was used to measure the x-, y-, and z-location of the first reference point (ball) on the CRD. This procedure was then repeated for the other two reference points. The above steps were then repeated for each posture in the data collection run.

Static calibration data collection run number I was used to establish a baseline for the succeeding calibration runs. The CMA was oriented randomly relative to the manipulator. The zero location and the axis orientation of the CMA were used to

establish the origin and axis orientation, respectively, of the global coordinate system used for manipulator calibration. Manipulator zero-point adjustment and calibration data collection were both carried out after manipulator warm-up.

For static calibration data collection run number II, the origin of the zero-point of the CMA (and therefore the origin of the global coordinate system) was shifted by a small amount, effectively changing the paramaeters which describe the first link on the manipulator kinematic model. A calibration data collection run was then made to see if the calibration algorithm could detect this change of parameters. Again, zero-point adjustment and data collection were both carried out after manipulator warm-up.

As stated previously, manipulator warm-up characteristics have been shown to have an important effect on manipulator accuracy [24,25]. To test the capability of the calibration algorithm to detect parameter changes due to warm-up, a third calibration data collection run was made in which the GE A4 was zero-adjusted cold and data was collected after warm-up. The same CMA zero location was used as in static calibration data collection run number II.

It is important for the detection of manipulator damage or wear that the calibration algorithm be able to detect parameter changes due to permanent link deflection. To test for this capability, a horizontal external force of five pounds was applied to the manipulator at the end effector, as shown in Figure 2.7. This force served to cause a relatively consistent deflection of the end effector and associated manipulator components. A fourth data collection run was made with this five-pound force acting during all measurements. Zero-point adjustment and data collection were both carried out after manipulator warm-up.

For each of the data sets resulting from the data collection runs described above, several static calibration cases were investigated. These cases differ only in the parameter set chosen for optimization. They were run to investigate the effects of including or not including particular parameters in the numerical synthesis. Parameters

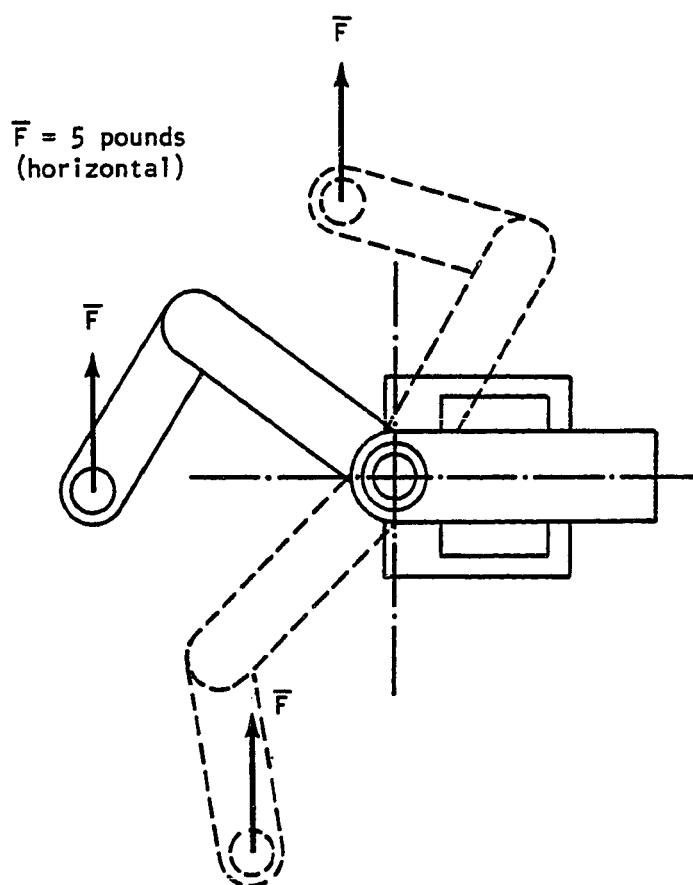$\overline{F}$ = 5 pounds
(horizontal)

Figure 2.7: Orientation of the External Five-Pound Force (Top View)

optimized for each of the various cases within each of the various data collection runs are listed in Table 2.1.

2.3.5.3 Results and Discussion

The preliminary experimental runs established or confirmed several characteristics of the robot and the CMA:

1. CMA repeatability was established at ±0.001 inches. This value was considerably better than manipulator accuracy, which was estimated to be ±0.300 inches.

2. Manipulator repeatability was established at ±0.002 inches when the target pose is always approached along the same path, ±0.008 inches if the target pose is approached along random paths. (Note that the manufacturer's repeatability specification of ±0.002 inches assumes uni-directional approach.)

3. End effector position error due to manipulator warm-up effects was established at ±0.010 inches, which confirmed the importance of the effect of warm-up on end effector positioning accuracy.

Estimates of 16 synthesized parameters at various iterations are shown in Table 2.2 for a typical optimization sequence using 36 calibration postures and the numerical partial derivative formulation. The 36 static calibration postures are shown schematically in Appendix B. The results of Table 2.2 clearly demonstrate the strong convergence typically expected within three or four iterations. Failure of the numerical partial derivative algorithm to converge within six iterations has proven to be an indicator of various manipulator mechanical or electrical malfunctions or of human data collection error. Additionally, this data indicates that (1) the parameters are steady at convergence (with the exception of the redundant parameters, discussed below), (2) the objective function (the sum of the squares of the residuals between measured and calculated poses) drops dramatically after the first iteration, as expected,

Table 2.1: Optimized Parameter Cases

Parameter Name	Number	Case 1	2	3	4	5	6	7	8	9
a_1	1	yes	yes	yes	yes	yes	no	no	no	no
b_1	2	yes	yes	yes	yes	yes	no	no	no	no
c_1	3	yes	yes	yes	yes	yes	no	no	no	no
α_1	4	no	no	no	no	no	no	no	yes	yes
β_1	5	no	no	no	no	no	yes	yes	yes	yes
γ_1	6	no	no	no	no	no	yes	yes	yes	yes
a_2	7	yes	yes	yes	yes	yes	no	no	no	no
b_2	8	yes	yes	yes	yes	yes	no	no	no	no
c_2	9	yes	yes	yes	yes	yes	no	no	no	no
α_2	10	no	no	no	no	no	no	no	no	yes
β_2	11	no	no	no	no	no	yes	yes	no	yes
γ_2	12	no	no	no	no	no	yes	yes	no	yes
a_3	13	yes	yes	yes	yes	yes	no	no	no	no
b_3	14	yes	yes	yes	yes	yes	no	no	no	no
c_3	15	yes	yes	yes	yes	yes	no	no	no	no
α_3	16	no	no	no	yes	yes	no	no	no	no
β_3	17	no	no	no	yes	yes	yes	yes	no	no
γ_3	18	no	no	no	yes	yes	yes	yes	no	no
a_4	19	yes	yes	yes	yes	yes	no	no	no	no
b_4	20	yes	yes	yes	yes	yes	no	no	no	no
c_4	21	yes	yes	yes	yes	yes	no	no	no	no
α_4	22	no	no	no	no	yes	no	no	no	no
β_4	23	no	no	no	no	yes	yes	yes	no	no
γ_4	24	no	no	no	no	yes	yes	yes	no	no
a_5	25	yes	yes	yes	yes	yes	no	yes	no	no
b_5	26	yes	yes	yes	yes	yes	no	yes	no	no
c_5	27	yes	yes	yes	yes	yes	no	yes	no	no
α_5	28	no	no	yes	yes	yes	no	no	no	no
β_5	29	no	no	yes	yes	yes	yes	yes	no	no
γ_5	30	no	no	yes	yes	yes	yes	yes	no	no
θ_{01}	43	yes	yes	yes	yes	yes	yes	yes	yes	yes
θ_{02}	44	yes	yes	yes	yes	yes	yes	yes	yes	yes
θ_{03}	45	yes	yes	yes	yes	yes	yes	yes	yes	yes
θ_{04}	46	yes	yes	yes	yes	yes	yes	yes	yes	yes
k_1	49	yes	no	no	no	no	no	no	no	no
k_2	50	yes	no	no	no	no	no	no	no	no
k_3	51	yes	no	no	no	no	no	no	no	no
k_4	52	yes	no	no	no	no	no	no	no	no

Table 2.2: Typical Parameter Convergence, Calibration Data Collection Run I, Case 5
(36 Postures)

Parameter	Initial Estimate	First Iteration	Second Iteration	Third Iteration, Convergence
a_1 (in)	15.080	15.332	15.332	15.332
b_1 (in)	-8.500	-8.243	-8.243	-8.243
c_1 (in)	10.540	10.612	10.615	10.613
a_2 (in)	0.000	0.000	0.006	-0.014
b_2 (in)	15.750	15.747	15.749	15.749
c_2 (in)	0.000	-0.072	-0.075	-0.073
a_3 (in)	0.000	-0.028	-0.030	-0.046
b_3 (in)	11.810	11.778	11.760	11.775
c_3 (in)	0.000	-0.072	-0.075	-0.073
α_3 (deg)	0.000	-0.874	-2.342	-2.285
β_3 (deg)	0.000	-0.100	-0.097	-0.096
γ_3 (deg)	0.000	0.083	0.087	0.087
a_4 (in)	0.000	-0.004	-0.028	-0.004
b_4 (in)	0.000	-0.009	0.008	-0.006
c_4 (in)	1.500	1.425	1.427	1.442
α_4 (deg)	0.000	-0.875	0.554	0.759
β_4 (deg)	0.000	-0.183	-0.181	-0.181
γ_4 (deg)	0.000	-0.257	-0.263	-0.266
a_5 (in)	0.875	0.881	0.882	0.882
b_5 (in)	-0.125	-0.134	-0.133	-0.129
c_5 (in)	3.000	2.931	2.937	2.946
α_5 (deg)	171.000	170.707	170.726	170.981
β_5 (deg)	0.000	-1.126	-1.126	-1.126
γ_5 (deg)	90.000	89.531	89.530	89.530
θ_{01} (deg)	90.000	88.885	88.906	88.834
θ_{02} (deg)	-117.000	-115.405	-115.546	-115.439
θ_{03} (in)	0.250	0.143	0.143	0.113
θ_{04} (deg)	200.000	199.237	199.378	198.826
SSQ	18.29916	0.10567	0.10512	0.10510
σ	0.29106	0.02212	0.02206	0.02206

Position Residual Deviation: σ_r = 0.03071 in
Attitude Residual Deviation: σ_ϕ = 0.00549 rad

and (3) projected improvement in average pose accuracy is substantial, as indicated by the change in mean residual deviation σ.

Comparisons of final estimates for two typical parameters over the several data collection runs/parameter estimation cases are shown in Figures 2.8 and 2.9. These figures show that, for the same manipulator/CMA configuration, the number of parameters estimated has only a minor effect on the value estimated for any particular parameter. These figures also demonstrate that the parameter estimation algorithm is capable of detecting several mechanical and electrical conditions, including CMA origin shift (runs I and II), manipulator warm-up effects (runs II and III), and link deformation/external loading (runs III and IV).

Existence of redundant parameters in the GE A4 and therefore in the estimation algorithm proved to be the most serious consideration in interpretation of the final parameter estimates. Although estimations involving various redundant parameters were successful using both derivative formulations, significantly weaker convergence was observed as compared to solutions for parameter sets with a low degree of redundancy. The redundant parameters tend to interact with one another even at a minimum objective function evaluation and continue to numerically wander, producing non-unique solutions for these particular parameters, as expected.

Parameters which are redundant at *each* measured posture (as opposed to a limited number of postures or posture regions) will create problems in the inversion of $[X]^T[X]$, in that these redundant parameters cause two (or more) columns of the matrix $[X]^T[X]$ to be (theoretically) identical. In actual practice, however, errors inherent in the data collection process and numerical techniques used by the Marquardt algorithm usually allow inversion of this matrix, leading to a useful solution. Even in the absence of redundant parameters, the matrix $[X]^T[X]$ is typically ill-conditioned due to inherent manipulator geometric properties or, to a lesser extent, an unwise choice of physical units for the various elements of the Jacobian matrix $[X]$. Appendix C shows typical matrices $[X]^T[X]$ with and without redundant parameters.
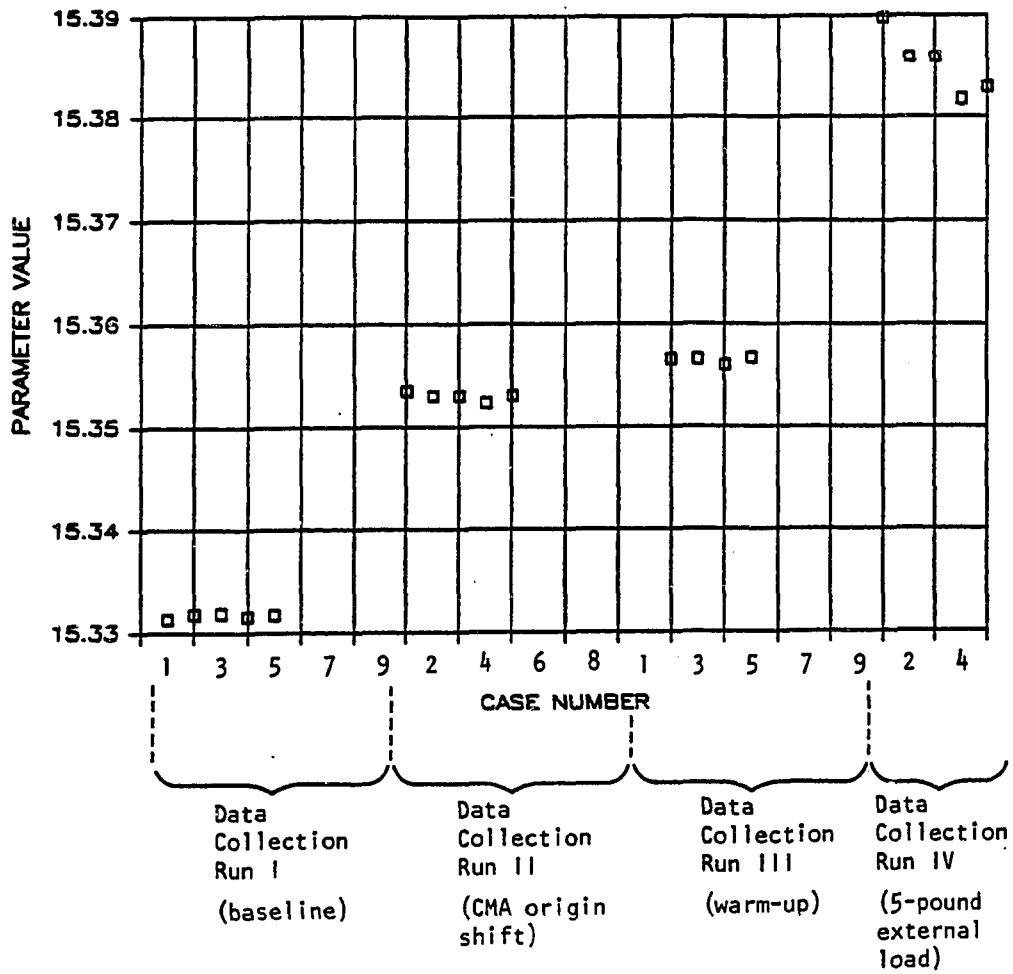
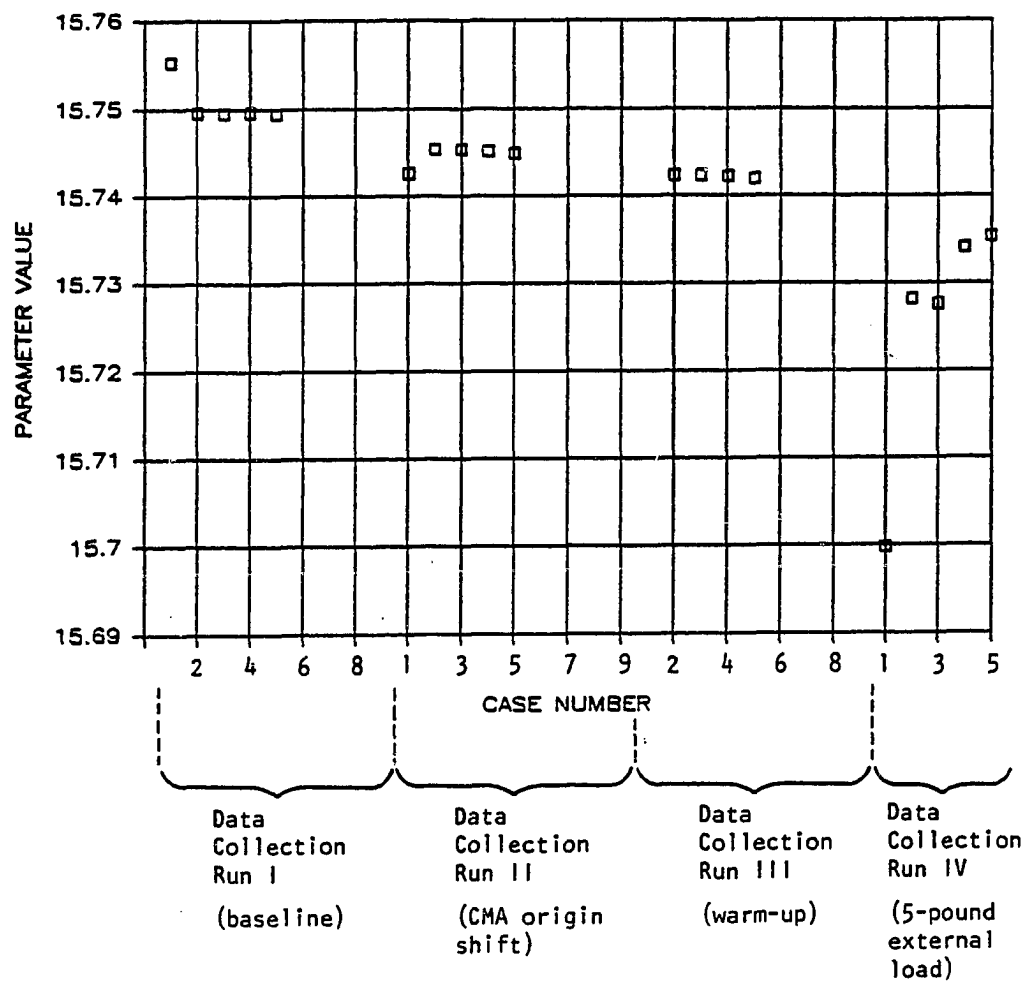Figure 2.8: Comparison of Final Parameter Estimates, Parameter 1 (Base X-Dimension, a_1)

Figure 2.9: Comparison of Final Parameter Estimates, Parameter 8 (Upper Arm Longitudinal Dimension, b_2)

Even small changes in parameter estimates as calculated by this technique have produced substantial improvements in manipulator aggregate error over the calibration field data. Although the sum-of-the-squares of the residuals is actually used as the objective function to be minimized by the algorithm, the square root of the normalized sum-of-the-squares, defined in Equation 2.12, provides a better indicator of manipulator positioning accuracy. This value may be viewed as the magnitude of the mean residual expected for any position or attitude measurement at any calibration point. Separating the sum-of-the-squares of position and attitude residuals and forming similar root-mean values, as shown in Equations 2.13 and 2.14, will produce separate estimates of the mean residual expected for position measurements σ_r and the mean residual expected for attitude measurements σ_ϕ.

$$\sigma = (SSQ/6n)^{1/2} \tag{2.12}$$

$$\sigma_r = (SSQ_r/3n)^{1/2} \tag{2.13}$$

$$\sigma_\phi = (SSQ_\phi/3n)^{1/2} \tag{2.14}$$

2.4 Conclusions

Distributions of final residuals for various calibrations have consistently demonstrated that the two mean residual values σ_r and σ_ϕ may be used as very good estimates of the standard deviations expected for any position or attitude quantity measured at the calibration points. Histograms of the residuals of the parameter estimation data presented in Table 2.2 are shown in Figures 2.10 and 2.11, with the corresponding Gaussian distributions superimposed for purposes of comparison. These histograms demonstrate approximate normal distributions, but more importantly show that (1) the distributions are not bi-modal, and (2) all residuals generally fall within plus or minus three standard deviations of the mean. In fact, 95 percent or more of the residuals will typically fall within plus or minus two standard deviations of the mean. The three groups of position residuals for r_1, r_2, and r_3, respectively, were pooled for these histograms, since the separate standard deviations and distributions of

σ_r=0.01773 in
36 postures
(108 samples)
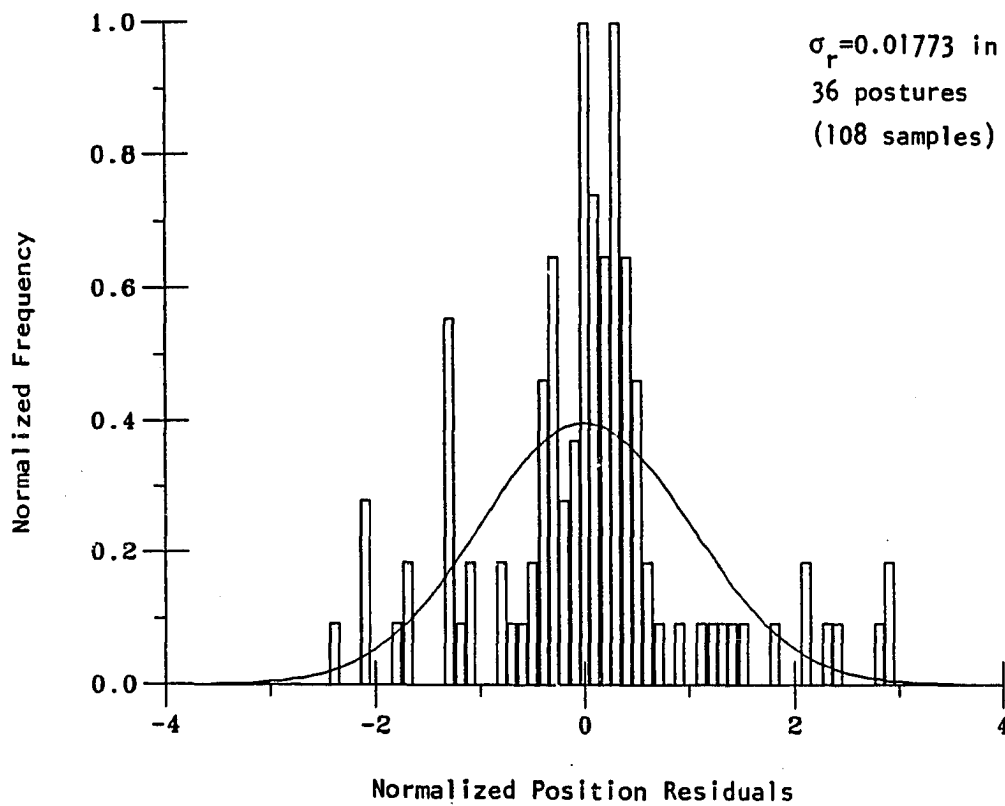
Figure 2.10: Typical Histogram of Final Position Residuals, Calibration Data Collection Run I, Case 5

σ_{ϕ}=0.00317 in
36 postures
(108 samples)

Normalized Frequency

Normalized Attitude Residuals
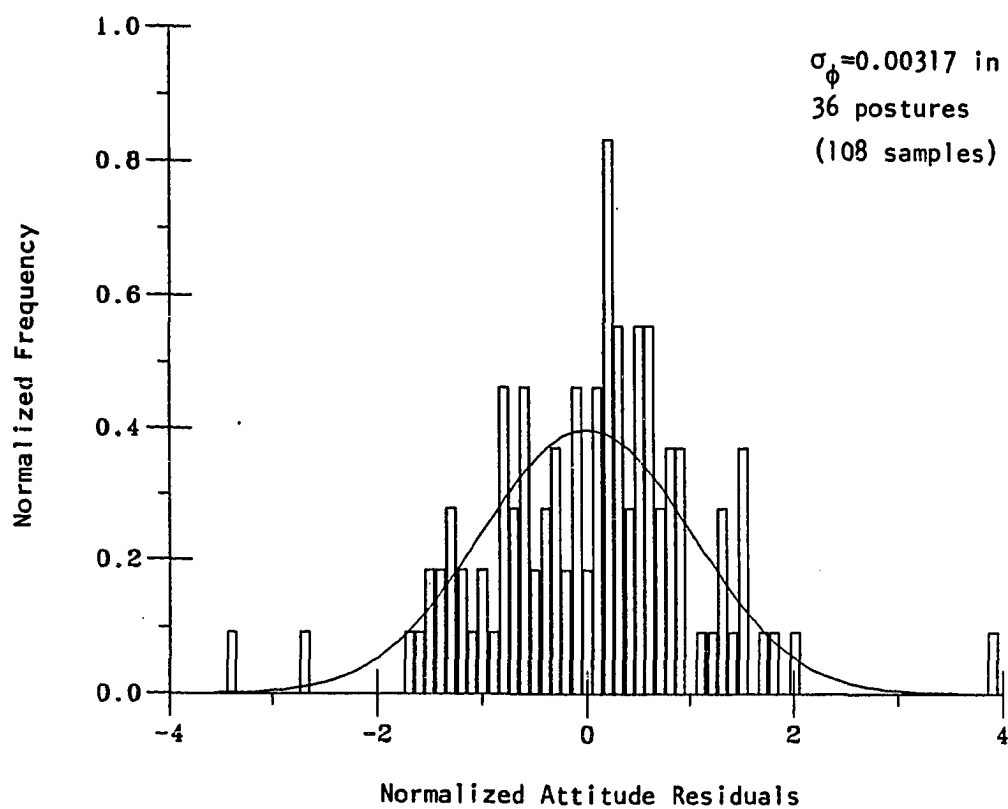
Figure 2.11: Typical Histogram of Final Attitude Residuals, Calibration Data Collection Run I, Case 5

the individual groups are commonly equivalent. The three groups of attitude residuals for ϕ_1, ϕ_2, and ϕ_3 were pooled in a like manner.

If the mechanical calibration points have been selected to sufficiently populate and span the desired manipulator workspace, then the σ_r and σ_ϕ values after calibration may also be used as good approximations to the standard deviations expected for the various manipulator positioning quantities (radial vector component or Euler angle) *anywhere* within the manipulator workspace. Similarly, the set of optimized parameter values may be used as a good approximation to that set which will miminize manipulator positioning error anywhere within the workspace. This approach (use of many more calibration postures than required and a least-squares approach to optimization) is in direct contrast to those methods which attempt to employ only the minimum number of calibration postures, producing estimated parameters which may increase manipulator positioning accuracy only in limited posture regions.

The above calibration technique can only improve the accuracy of the kinematic model of a particular manipulator and thus can remove only systematic errors in the manipulator positioning calculations. Although the technique can account for mean static bearing compliance and link flexure averaged over the calibration range of motion, random errors due to linkage component precision and lack of rigidity along with transducer signal acquisition error will still be present. This calibration technique only allows more accurate calculation of manipulator position and cannot improve either the mechanical or electrical accuracy of bearings, sensors, actuators, etc.

The GE A4 manipulator employs 500 pulse-per-revolution optical encoders for sensing of joint displacement. (Through the gear reducers, this translates into 50,000 pulses per revolution of the arm links.) Although these sensors exhibit quantization effects, their output may be assumed to be perfectly linear, as was done in the sample calibrations. Should nonlinearities become significant, as may occur in cases where potentiometers, synchros, or resolvers are used for position sensing, a polynomial approximation to the transducer calibration curves could easily be incorporated into the

above estimation scheme simply by fitting the additional transducer parameters along with the linear terms during the numerical optimization.

Redundant parameters in the manipulator mathematical model have been shown to complicate interpretation of estimated parameter values. Redundant parameters can normally be identified by one of the following types of behavior:

- Redundant parameters mutually interact with one another independently of the other parameters in a calibration set. This is demonstrated in Table 2.2, where parameters c_2 and c_3 are consistently adjusted to the same values at each iteration.

- At solution convergence, the algebraic sum of the values of a set of redundant parameters will remain constant even though the individual parameters wander numerically.

During the calibration process, the problem of redundant parameters can be remedied to various degrees by one or more of the following methods:

- Increase the number of calibration postures, the excursion of the joint variables during the calibration run, or both. This approach will work if certain parameters are redundant only near particular postures or within limited posture regions.

- Include (along intermediate manipulator links) multiple calibration sites per calibration posture, as discussed in Section 2.3.1.

- Optimize only one parameter of a set which is known to be redundant.

If desired, analysis of variance in the parameter updates may be accomplished by noting [26] that the variance-covariance matrix for the update vector $\{\beta\}$ is given by

$$[V_\beta] = ([X]^T[X])^{-1} \sigma^2 \qquad (2.15)$$

for any particular iteration. The variance-covariance matrix for the final optimized parameters, then, would be obtained by summing the variance-covariance matrices for each level of updates.

Research objectives met in this chapter include:

1. design of an algorithm to carry out the static calibration of a robotic manipulator,

2. numerical implementation of the static calibration algorithm,

3. testing of the static calibration algorithm via numerical simulation of various robots, and

4. testing of the static calibration algorithm using data from a real industrial robot.

2.5 Summary

This chapter presents a general, flexible, efficient approach to static kinematic parameter estimation for calibration of robotic manipulators. The combination of external measurement, numerical kinematic synthesis, and manipulator kinematic model correction allows regressive re-evaluation of selected elements in the parameter set which analytically describes such manipulators. Use of these synthesized parameter estimates permits significantly more accurate positioning of a point or points on a manipulator. The technique also produces an approximate statistical prediction of the accuracy of such positioning throughout the mechanical calibration space. Predictive maintenance and repair of manipulators will also be important practical application areas for the static calibration procedure.

Chapter 3

VIBRATIONAL CALIBRATION

3.1 Introduction

In Section 2.1 it was shown that static positioning accuracy is an important performance criterion for robotic manipulators. Clearly, the accuracy of a robotic manipulator is also dependent on the characteristics of its structural vibrations, which are, in turn, posture-dependent. (In the context of this work, "vibration" will be taken to mean "small oscillation about an equilibrium structural posture," which is similar to the definition used by Uicker [27].) Vibrations from several sources along the manipulator's kinematic chain sum to produce a vibration at the end effector coordinate frame (EECF). Conversely, if the vibrations of the EECF are known, they may be decomposed into vibrations of the various manipulator components (parameters) using extensions of the same techniques as those used in the static closure process. Re-evaluation, from a vibrational standpoint, of these parameters in a calibration scheme will provide a vibrational analytical description of each calibrated parameter. The resulting body of data may then be analyzed to determine which manipulator components are contributing most significantly to the EECF vibrations over the entire workspace of the manipulator. Such a description will be useful in improving vibrational manipulator accuracy and in implementing manipulator predictive maintenance strategies [28].

Such a calibration scheme may be formulated as a frequency-by-frequency dimensional synthesis of vibrational manipulator parameters based on data taken from

external mechanical measurements. The external mechanical data is obtained from a frequency analysis (via accelerometry) of the manipulator. This analysis produces frequency-domain vibrational information for each of the six spatial degrees-of-freedom at the measurement point. The frequency analysis is then repeated over a sufficient number of postures to representatively populate and span the manipulator's workspace. Next, a synthesis procedure, similar to that used in the static calibration, is performed at each discrete frequency value, producing frequency-domain descriptions of each of the parameters. The resulting optimal vibrational parameters will minimize, in a dynamic sense, manipulator end effector coordinate frame (EECF) positioning error over the selected calibration space.

From a kinematic standpoint, this calibration may be expressed as a multiple-point synthesis of a spatial open-loop mechanism for rigid-body guidance at each discrete frequency value in the range of interest. This vibrational kinematic calibration offers many of the benefits of a multiple-posture modal analysis at substantially reduced cost in both data collection and processing time. To date, no studies have been published which explore this facet of the vibrational kinematic calibration algorithm for movable structures (e.g., robots).

From a practical standpoint, the body of parameter data generated by a vibrational calibration will be very useful in identifying and isolating points of damage or wear before such problems might become discernible by other means. If a vibrational calibration is performed on a particular robotic manipulator at regular time intervals (every month, for instance), then the values of the various parameters can be compared to their corresponding values during previous tests, for the purpose of identifying those parameters whose vibrational characteristics are changing more than an acceptable or expected amount. (When applied in this way, the vibrational calibration data is part of a program known as predictive maintenance.) After additional experience with the vibrational calibration procedure, it will be possible to make specific maintenance or repair recommendations for a manipulator on the basis of its vibrational calibration history.

3.2 Kinematic Modeling

The fundamental task of a robotic manipulator is to deliver its end effector to a known position and attitude relative to a fixed, pre-defined coordinate frame. This relationship between the moving (end effector) coordinate frame and the fixed (base) coordinate frame may be affected not only by static inaccuracies within the manipulator, but also by vibrational inaccuracies and inconsistencies. Through vibrational kinematic parameter estimation, vibrational displacements at a particular site on a manipulator may be decomposed into variations in the individual manipulator parameters (describing discrete hardware components).

A description of the vibrational characteristics of any desired site on the manipulator may be obtained through frequency response analysis (also known as Fourier analysis or spectral analysis). Through frequency response analysis, spectral transfer functions may be obtained which relate vibrational outputs at any given site to vibration-inducing inputs at any other given site on the manipulator. Assuming a linear physical system, the transfer function is defined as a complex-valued function in the Laplace domain, and has the general form

$$H(s) = X(s)/F(s) \quad , \tag{3.1}$$

where $X(s)$ represents the Laplace transform of the system output and $F(s)$ represents the Laplace transform of the system input. Figure 3.1 shows a three-dimensional graph of a typical single-degree-of-freedom transfer function. The frequency response function for a system input/output pair is obtained by evaluating the (complex-valued) transfer function for that pair along the $j\omega$ (frequency) axis.

If desired, the data collected during the frequency response analysis may be used as input to modal analysis. Using modal analysis, several important dynamic characteristics of a structure may be extracted from the structure's frequency response data, including the natural frequency, mass coefficient, damping coefficient, stiffness
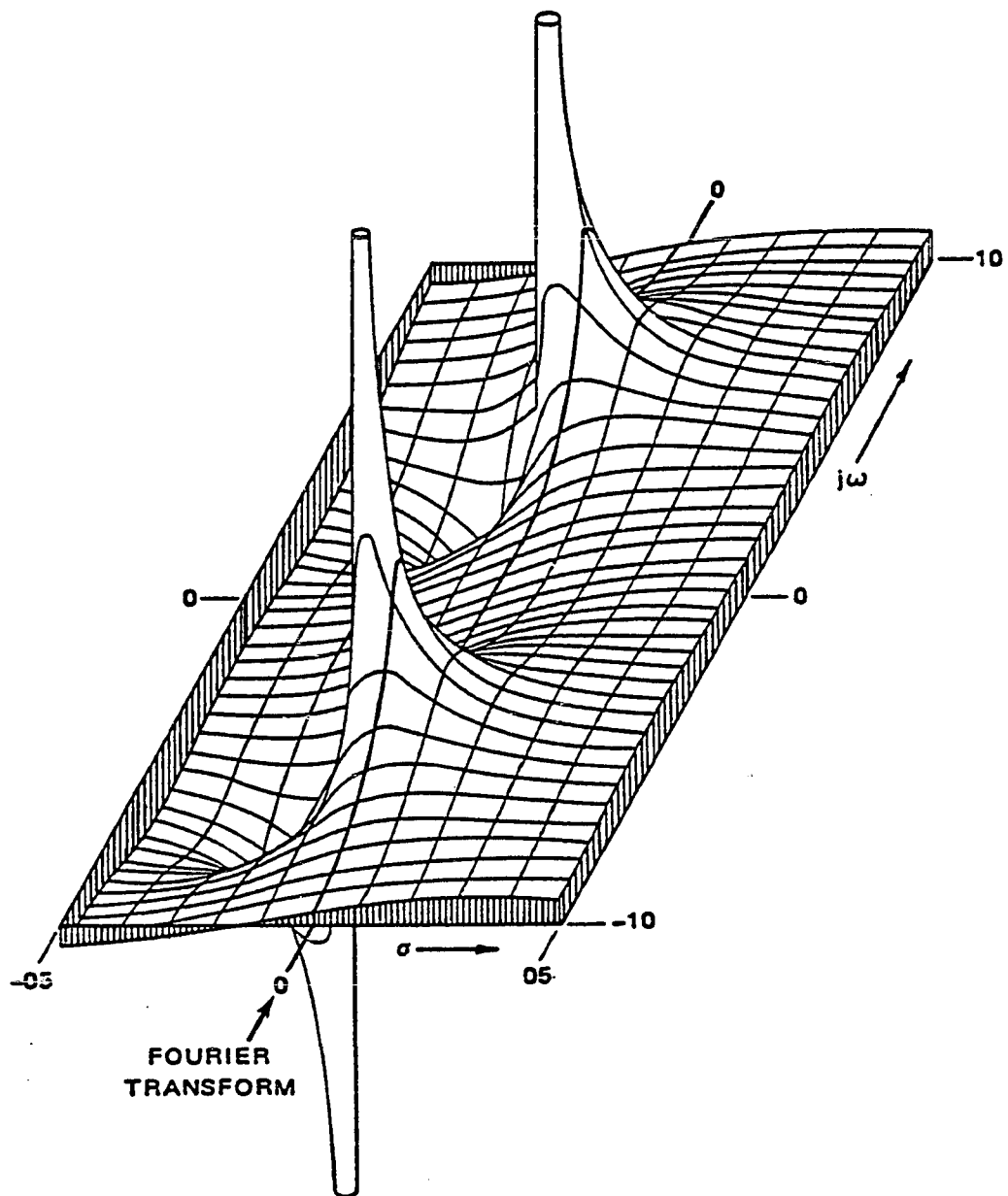
Figure 3.1: Real Part of the Transfer Function of a Single-Degree-of-Freedom System with Poles at s=-1±j5

coefficient, and characteristic mode shape of each of the structure's modes of vibration. Once the dynamic properties of a structure have been determined, its behavior may be predicted and, therefore, controlled and optimized.

As dynamic systems, robotic manipulators tend to be significantly nonlinear due to joint compliance, joint backlash, load-sensitive stiffness, Coulomb damping, and other types of nonlinear damping. Therefore, it is important to consider the various types of nonlinearities which can occur in dynamic systems, and to be able to identify nonlinearities in frequency response functions [29]. Kirshenboim and Ewins [30] have proposed a method for recognizing structural nonlinearities in frequency response analysis which may be useful for this purpose.

There are several areas where errors affecting vibrational manipulator accuracy may appear in this model. The most suspect areas are in the determination of the physical parameters. Although mechanical components may be accurately machined, gauged, and assembled in the laboratory, link flexure or permanent deformation, joint compliance, component wear, and manipulator field assembly/modification may make exact knowledge of certain individual parameter values nearly impossible. Parameter values which change over large intervals of time (months, years) due to wear, corrosion, creep, stress relaxation, or other effects may be particularly difficult to detect at an early stage with static techniques. It is a purpose of this work to describe a method for the numerical estimation of such parameters based on a carefully performed mechanical vibrational calibration of a fully assembled robotic manipulator.

3.3 Calibration

3.3.1 Measurement

The mechanical vibrational calibration should place the moving and fixed ends of the manipulator in several exactly known relative positions and attitudes at which system input/output characteristics can be measured. (Typically, data for the static and vibrational calibrations can be collected at the same time.) Input excitation of the manipulator structure is typically a known forcing function applied at a selected point. This force may be provided by any of several means, including instrumented hammers and electrodynamic or mechanical shakers. Whichever method is chosen, a force transducer positioned between the exciter and the structure usually provides data on the actual force applied by the exciter to the structure. Typical system output is an acceleration at a selected point, measured by any of a wide range of commercially available accelerometers.

At each of the poses above, appropriate force input and acceleration output data should be collected for calculation of the six corresponding frequency response functions, one each for the three translational and the three rotational degrees-of-freedom. Accumulation of these frequency response measurements at several postures will allow re-evaluation of the final static calibration values of the various physical and electrical parameters to produce time- or frequency-domain vibrational descriptions of these same parameters.

The same types of alternatives to the measurement of rotational data apply in the vibrational case as do in the static case. That is, linear vibrations of three (or more) non-collinear sites on the component of interest may be measured instead of three rotational vibrations. This multiple-site linear vibration data may then be either converted immediately to an angular form or input directly into the vibrational calibration algorithm in the form of additional calibration points.

In obtaining frequency response function data, it is important to know as much as possible about the range of frequencies in which the first several modes of vibration will occur. Approximate knowledge of this range allows the choice of an experimental frequency band such that resolution in the frequency response functions will be as high as possible while still covering the expected frequency range. Also, if the upper frequency of interest can be identified, appropriate anti-aliasing filters may be applied to the input and output signals. Preliminary studies by Stoltzfus and Young [31] and Berger, Fessler, and Kaylor [32] have identified the frequency ranges of interest for two common industrial robots (a General Electric P50 and a General Electric A3, respectively), and have presented several useful observations on the frequency response testing procedure as it applies to robotic manipulators. Based on these two reports, the following observations and predictions concerning the frequency response testing of typical small- to medium-sized robotic manipulators can be made:

1. the first several vibrational modes will occur below 100 Hertz,

2. impulse testing is poorly suited to these measurements due to the large sample time necessary to obtain acceptable frequency resolution over a band of zero to 100 Hertz, and

3. equipment used to excite the manipulator must have better-than-average low-frequency power and response characteristics in order to impart sufficient low-frequency energy to the manipulator.

In a practical experimental situation, frequency response analysis is usually accomplished with the help of a digital Fast Fourier Transform (FFT) analyzer. A digital FFT analyzer will perform or aid in the performance of several steps in the frequency response analysis, including data collection, analog-to-digital conversion, FFT implementation, and frequency response function calculation and display. If desired, the analyzer will also aid in the performance of several of the steps required for modal analysis, including model definition, mode shape identification, and modal parameter extraction.

Several types of excitation signals are in common use for frequency response testing, including pure random, pseudo-random, periodic random, sinusoidal, impact, and step relaxation. Choice of a particular type of excitation is dependent upon the characteristics of the structure under test. The only requirement on excitation functions is that they contain energy at all frequencies within the measuring range of interest.

In cases where the test structure is significantly nonlinear, periodic random excitation is often the most useful [33]. Periodic random waveforms combine the best features of the pure random and the pseudo-random waveforms:

1. the periodic nature of the random periodic waveform eliminates leakage effects in the FFT, and

2. the random nature of the periodic random waveform (the structure is subjected to a different excitation during each successive measurement) makes the use of ensemble averaging effective for removing noise and distortion from the frequency response function.

One effective and versatile means of generating a periodic random signal (or any of the random signals) is to synthesize the signal in software on a digital computer or in hardware in a dedicated digital circuit, and subsequently pass the signal to the exciter via a digital-to-analog converter.

3.3.2 Identification

As in the static calibration, the identification portion of the vibrational calibration scheme may be formulated as a nonlinear optimization of the manipulator's physical and electrical parameters. The static measures of joint transducer voltages at each calibration posture may be viewed as the function generator input vector. The radial vector components and Euler angles calculated by the manipulator kinematic model (based on optimal static parameter estimates and the input vector) may be viewed as the estimated function generator output vector. The exactly known

vibrational spectra of the radial vector components and Euler angles at each mechanical calibration posture consist of that portion due to the static pose of the end effector and that portion due to the vibrational deflection of the end effector; the sum of these portions may be viewed as the desired function generator output vector. The manipulator's physical parameters correspond to the mechanism link dimensions.

The principal conceptual difference between the static and vibrational parameter estimations lies in the form of the estimated parameters. In the static calibration, parameters took on scalar values. In the vibrational calibration, however, each parameter represents a dynamic quantity, and must therefore be described by a frequency spectrum or equivalent form. These synthesized spectra are frequency response functions (FRFs) which relate the vibrations of the associated parameter (manipulator component) to the system input vibrations.

The optimization process described above must synthesize a set of spectra for the manipulator's physical and electrical parameter estimates which produce the best possible function generation as described by an aggregate measure of the difference in desired and calculated output vectors over all calibration points. As in the static calibration, this process may be done iteratively by evaluating the aggregate function generation error for an estimated parameter set, and, based on various gradient and search techniques, minimizing that aggregate error through simultaneous modifications of the several parameter estimates. However, since the vibrational data typically represent very small-amplitude displacements, the vibrational calibration optimization process may be approximated by using the linear Jacobian relationship

$$\{Y\} = [X]\{\beta\} \quad , \tag{3.2}$$

where [X] represents the Jacobian matrix from the final iteration of the Marquardt static calibration, {Y} the vector of EECF vibration spectra, and {β} the vector of corresponding parameter vibration spectra. (Note that, based on the expanded form of [X] shown in Equation 2.11, the Jacobian is not frequency-dependent.)

The goal of the analysis described above is prediction of vibrational displacements of the EECF for several combinations of system excitations and configurations. When EECF vibrational displacement is known for any particular system excitation/configuration, vibrational transfer functions for the individual manipulator components (parameters) may be found by solving the matrix Jacobian equation

$$\{\beta\} = ([X]^T[X])^{-1}\,([X]^T\{Y\}) \quad . \tag{3.3}$$

Although the approach of Equation 3.3 parallels the iterative solution scheme of the static calibration, the vibrational calibration is linear, owing to the assumed very small displacements represented by {Y} above.

In the vibrational realm, Equation 3.3 may be applied separately to both the real and the imaginary portions of the EECF vibrational data at each spectral line. This approach directly produces a set of parameters which are described in terms of their real and imaginary parts at each discrete frequency of the experimental vibrational spectrum.

As in the static calibration, weighting techniques may be used to reduce (or accentuate) the effects of various components of the vector of EECF vibrations {Y} in Equation 3.3. The coherence function, a measure of the quality of the experimental frequency response function at the various discrete frequencies, is one logical choice for determining weighting factors for the solution of Equation 3.3, and may be used as necessary.

3.3.3 Correction

From a correctional standpoint, the body of parameter data generated by the vibrational calibration will be very useful in identifying and isolating pending equipment failures (in a predictive maintenance sense) before the failures might become discernible by other means. If a vibrational calibration is performed on a particular robotic manipulator at regular time intervals (every month, for instance), then the behavior of the various parameters can be compared to their corresponding behavior during previous tests, for the purpose of identifying those parameters whose behavior is changing more than an acceptable or expected amount. After additional testing of and experience with the vibrational calibration procedure, it may be possible to make specific maintenance or repair recommendations for the manipulator under test on the basis of its vibrational calibration history.

Another approach to correction in the vibrational case parallels that of the static case; that is, to modify the control algorithm of the manipulator under test based on the results of the vibrational calibration. All of the procedures and requirements for correction in the static case apply equally well to the vibrational case. In addition, special mention must be made of the speed of execution of the control algorithm. Due to the high-frequency nature of the vibrational calibration data, correction could only be implemented in a controller with a relatively large response bandwidth. Limited bandwidth of the control systems and/or algorithms of current-generation robots would prevent the successful inclusion of vibrational calibration correction information.

3.3.4 Experimental Investigation

3.3.4.1 Apparatus

The vibrational parameter estimation algorithm was tested on a General Electric model A4 (GE A4) industrial robot. The test set-up consisted of four major parts: the robot itself, the robot control unit, the excitation system, and the measurement system. The GE A4 industrial robot and control unit used in the vibrational testing were the same as those used in the static testing, and are described fully in Section 2.3.5.1.

The excitation system was used to provide a controlled vibrational input force to the GE A4, and consisted of the components shown in Figure 3.2. The noise generator produced white noise with a frequency spectrum which was flat from 2 to 20,000 Hertz. Output from the noise generator was fed to an analog low-pass filter with variable cut-off frequency; this filter was used to limit the frequency content of the excitation signal to a range just slightly larger than the measurement region of interest, effectively allowing the signal amplifier's power to be restricted only to those frequencies within the region of interest. The filter output was fed to the power amplifier, which boosted the excitation signal to the level required by the electrodynamic shaker. The power amplifier had a low-frequency half-power point of 3 Hertz, and was the weakest link, with respect to low-frequency response, of all components of the vibrational excitation system. The shaker itself was capable of producing a 50-pound peak (sine) output, providing maximum accelerations of 0.2 g at 2 Hertz and 2.0 g at 20 Hertz, and was specifically designed for modal testing with a low-mass armature. The shaker provided force excitation at the robot's end effector during most measurements.

The measurement system, shown schematically in Figure 3.3, consisted of force and acceleration transducers, their associated electronic components and circuitry, and a fast Fourier transform (FFT) analyzer. The piezoelectric load cell was capable of measuring a maximum force of 500 pounds with a sensitivity of 5.73 mV/lb. The load
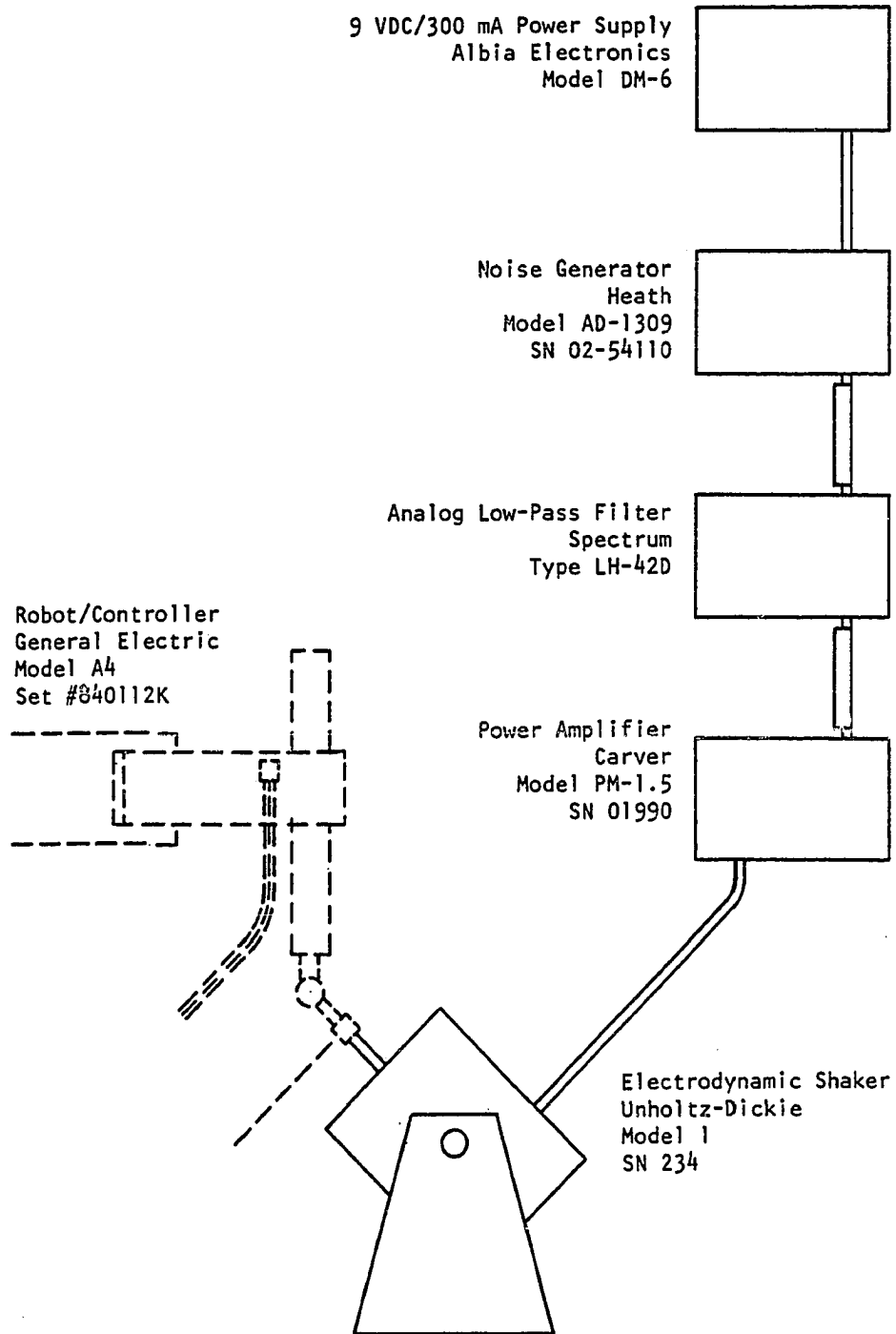
9 VDC/300 mA Power Supply
Albia Electronics
Model DM-6

Noise Generator
Heath
Model AD-1309
SN 02-54110

Analog Low-Pass Filter
Spectrum
Type LH-42D

Robot/Controller
General Electric
Model A4
Set #840112K

Power Amplifier
Carver
Model PM-1.5
SN 01990

Electrodynamic Shaker
Unholtz-Dickie
Model 1
SN 234

Figure 3.2: Schematic of the Vibrational Excitation System

Robot/Controller
General Electric
Model A4
Set #840112K

Force Transducer
PCB Piezotronics
Model 208A03
SN 4290

Triaxial Accelerometer
Entran
Model EGA3-1000D
SN 15T 4-2

12 wires

Power Unit
PCB Piezotronics
Model 480D06
SN 6518

Strain Gage Conditioners
Analog Devices
Model 2B31J
(3 in cabinet)

Multichannel FFT Analyzer
Zonic
Model 6080
SN 243

Real Time Display Terminal
Zonic
Model 6081
SN 210

±15 VDC/100 mA Power Supply
Analog Devices
Model 952

Color Monitor
Zonic
Model 6081 CM
SN 213

Figure 3.3: Schematic of the Vibrational Measurement System

cell had a discharge time constant of 2000 seconds and a resonant frequency of 70 kHz. The accelerometer was a triaxial, piezoresistive unit capable of measuring acceleration at levels up to ±1000 g's with a sensitivity of 0.25 mV/g. A Zonic FFT analyzer was used to capture dynamic data from both the load cell and the accelerometer; in addition, the analyzer performed anti-alias filtering, time-to-frequency domain conversion, calculation of autospectra and cross spectra for the various signal pairs, ensemble averaging, and calculation of coherence functions.

3.3.4.2 Procedure

Several stages of preliminary testing were undertaken to check characteristics of the robot and associated test systems. Specifically, tests were run to determine the effect on vibrational response of (1) the robot servo-control system, (2) input vibrational power, and (3) input direction (orientation), by varying each of these three parameters independently of the other two. In addition, a modal analysis was performed at one typical manipulator posture.

Several experimental runs were made to evaluate the effects of the manipulator servo-control system on manipulator vibrational response. This was necessary because the vibrational calibration algorithm was designed to estimate the vibrational properties of a manipulator's physical parameters, without regard to effects which may be introduced by the manipulator's servo-control system. In these test runs, inertance frequency response functions (FRFs) were measured alternately with servo-control system power on and with power off. These measurements were repeated at several representative postures throughout the manipulator's workspace.

According to linear frequency analysis theory [34], the level of power input to a structural system should have no effect on the measured system FRFs. As a check on this system characteristic, vibrational tests were run at several representative manipulator postures. At each of these postures, inertance FRFs were measured for each of several power amplifier gain settings.

Similarly, the direction (orientation) of the system input should have no effect on the measured system FRFs, provided that no coupling exists between the orthogonal axes of system output. (The latter condition is seldom satisfied in real manipulators.) To test for effects of input orientation, the GE A4 was moved to a typical posture near the center of the workspace. Here, inertance FRFs were measured for each of several orientations of the shaker armature axis. These orientations are illustrated in Figure 3.4.

In addition to the above stages of preliminary testing, a modal analysis was performed at one typical manipulator posture. Results from this modal analysis were used to provide a basis for (1) comparison to other investigator's results, and (2) evaluation of performance of the vibrational calibration algorithm. The 20 locations used in this modal analysis are shown in Figure 3.5, and the posture itself is shown in Figure 3.6.

The vibrational calibration data collection runs proceeded in a manner very similar to the static data collection runs. The vibrational calibration postures were a subset of those used for the static calibration, consisting of postures 5, 6, 7, 8, 17, 18, 19, 20, 29, 30, 31, and 32 as shown in Appendix B. At each calibration posture, induced vibrations of a point near the manipulator's end effector were measured in three dimensions. The FFT analyzer was used to simultaneously capture the one channel of force data and three channels of acceleration data, convert each signal to the frequency domain, form inertance frequency response functions (FRFs) relating each output acceleration to the input force, and perform ensemble averaging of the three FRF data sets. The final result of the measurement phase, then, was a set of inertance FRFs describing, in three dimensions, the vibrations of the manipulator's end effector at each of the calibration postures.

a) top view

A, B, and C horizontal
D, E, and F inclined
  at 45° from horizontal

b) end view
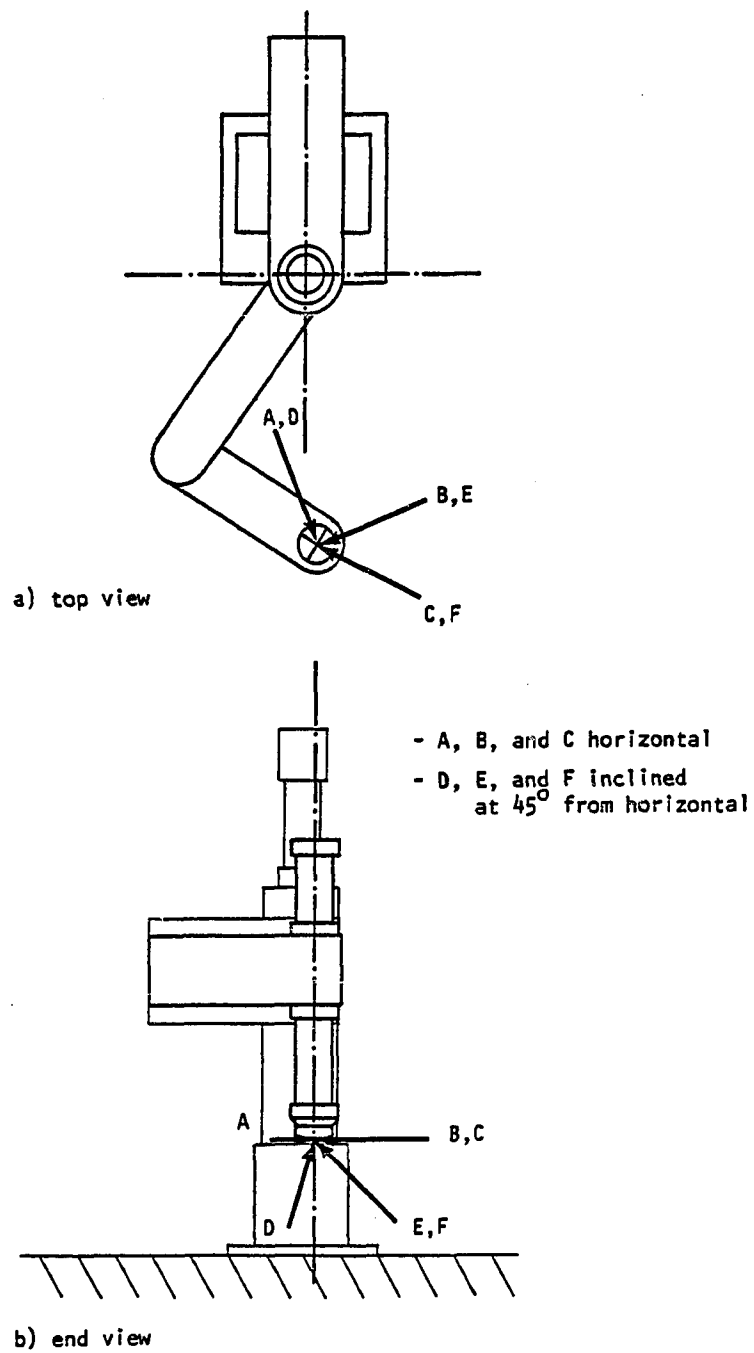
Figure 3.4: Orientations for Testing of the Effect of Input Orientation on Manipulator Vibrational Response
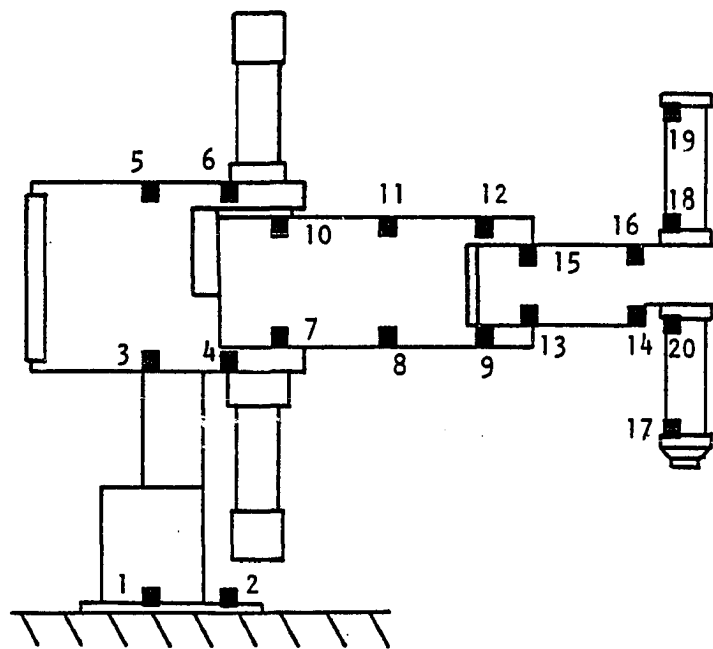
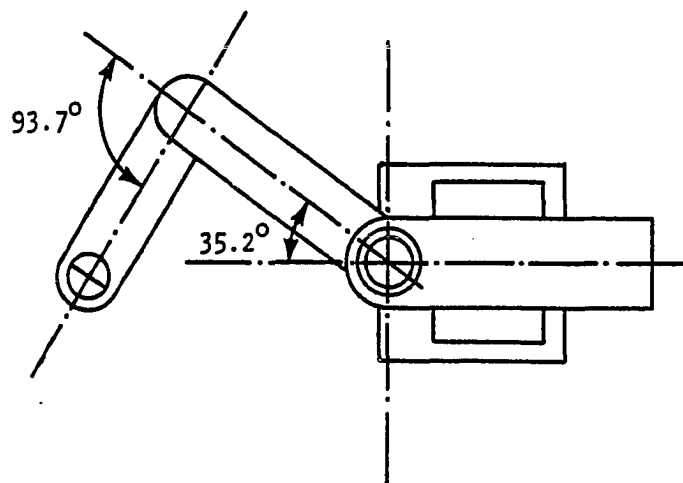Figure 3.5: Modal Analysis Accelerometer Locations (Side View)

Figure 3.6: Modal Analysis Posture (Top View)

3.3.4.3 Results and Discussion

The preliminary experimental runs established several characteristics of the experimental systems:

1. Figure 3.7 illustrates the difference between a typical "servos on" FRF and the corresponding "servos off" FRF. This figure shows that the effect of the manipulator servo system on vibrational response was very small: maximum separation between the two curves, excepting the region of the notch at 38 Hertz, is approximately 4 db in the 12-13 Hertz region; typical separation is less than 2 db.

2. Effect of input power level on vibrational response was also very small, as demonstrated by Figure 3.8. This figure shows inertance FRFs for three different input power levels for a particular response direction at a typical posture. Maximum separation between the three curves, excepting the region of the notch at 38 Hertz, is approximately 5 db in the 15-22 Hertz region; typical separation is less than 3 db.

3. The results of 1 and 2 above indicate that the GE A4, as a structural system, behaves linearly under a variety of conditions, and that previous assumptions of system linearity are justified; however, further results of preliminary testing show that orientation of the system input has a significant effect on system response. Figure 3.9 shows the FRFs measured at accelerometer location 16 (Figure 3.5) for a variety of input forcing orientations (Figure 3.4). This figure shows that input orientation does indeed have a significant effect on measured system FRFs: separation between the six curves shown runs between 10 and 40 db. This effect is not unexpected, since manipulators in general tend to be highly coupled structural systems. Further research is needed to determine the effects of input orientation on the results of a vibrational calibration and on manipulator frequency analysis in general.
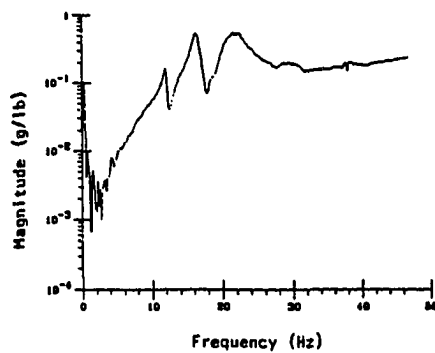
Magnitude (g/lb)

Frequency (Hz)

a) Servos On
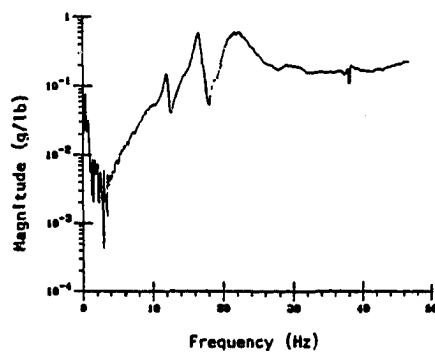
Magnitude (g/lb)
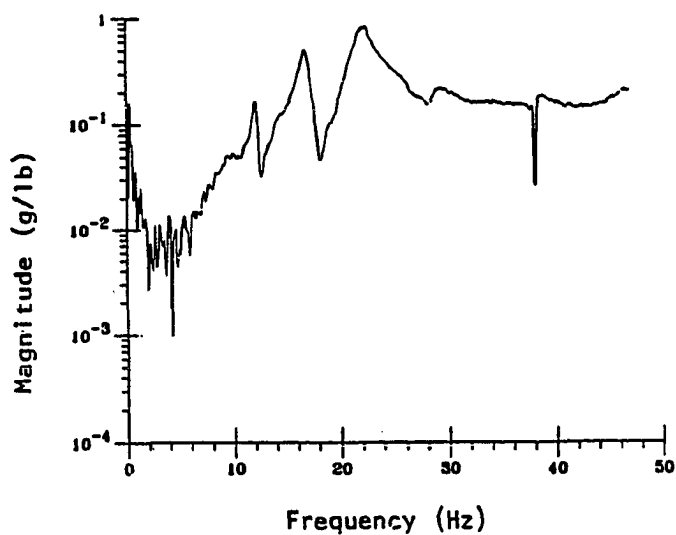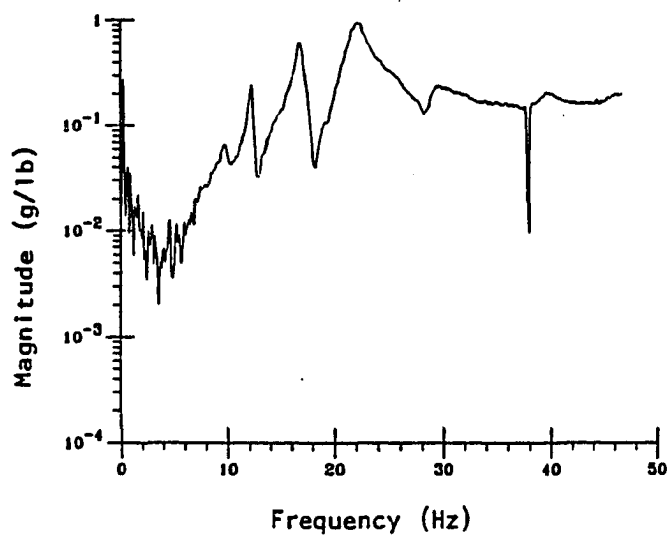
Frequency (Hz)

b) Servos Off

Figure 3.7: Typical Frequency Response Functions, Servos On/Off (Input Power Gain Setting -17.0 dB, Local Y-Direction Response, Accelerometer Location 16)
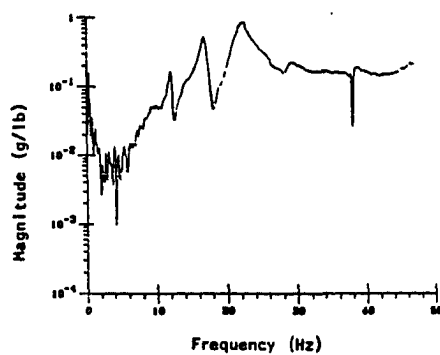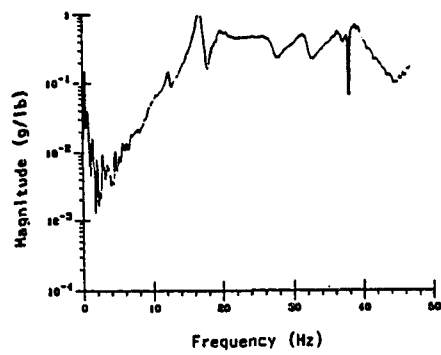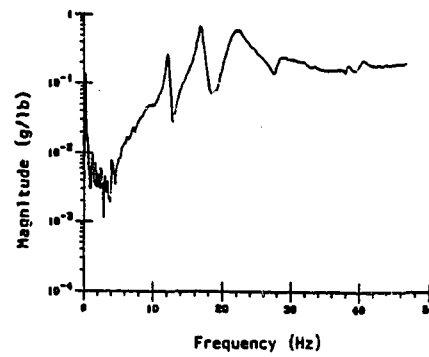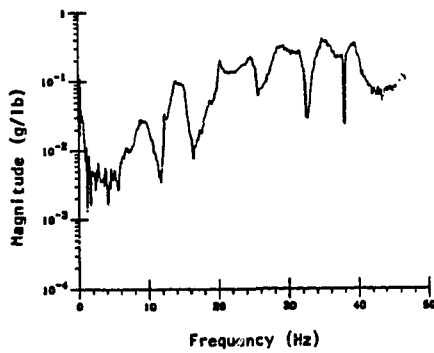
a) -4.8 dB

b) -9.3 dB

c) -17.0 dB

Figure 3.8: Typical Frequency Response Functions, Input Power Gain Settings -4.8 dB, -9.3 dB, and -17.0 dB (Servos On, Local Y-Direction Response, Accelerometer Location 16)
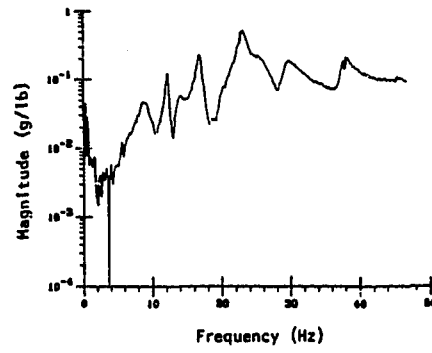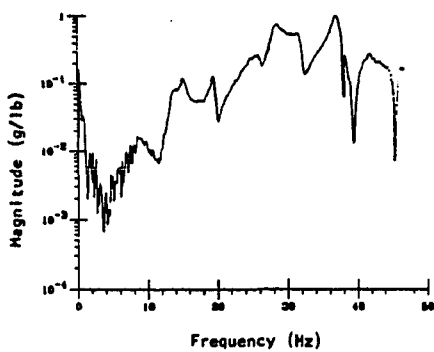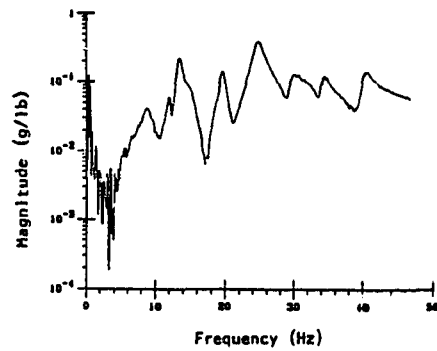
a) Orientation A

b) Orientation B

c) Orientation C

d) Orientation D

e) Orientation E

f) Orientation F

Figure 3.9: Typical Frequency Response Functions, Input Orientations A, B, C, D, E, and F (Input Power Gain Setting -9.3 dB, Servos On, Local Y-Direction Response, Accelerometer Location 16)

Many of the frequency response functions described by the figures above show a notch at approximately 38 Hertz. Although the cause of these notches is uncertain, they may be attributable to nonlinear Coulomb friction and deformation between gear teeth. Similar effects have been observed by Dagalakis and Myers [35]. Also, data below 3 Hertz in all of the above figures is meaningless, due to the low-frequency cutoff of 3 Hertz in the vibrational excitation system (described in Section 3.3.4.1). Coherence was acceptable (greater than 0.94) for all FRFs shown, excepting the immediate regions of peaks and notches and below 3 Hertz.

A modal analysis was performed for one typical manipulator posture, shown in Figure 3.6. The resulting first several modal frequencies are listed in Table 3.1. The first several modal frequencies and mode shapes are typical of a structure of this size and weight. The modal frequencies at 71 and 88 Hertz, however, showed significantly higher acceleration levels than the lower-frequency peaks. After viewing graphical displays of these mode shapes, it was determined that the vertical distal link of the GE A4 was vibrating essentially as a free-free beam, independently of the rest of the manipulator structure. This was possible because of the extreme difference in stiffness between the vertical link and the other links of the manipulator. The 71 Hertz mode was found to represent the lateral (with respect to the lower arm) first-mode vibration of the vertical link, and the 90 Hertz mode was found to represent the longitudinal (with respect to the lower arm) first-mode vibration of the vertical link.

Figure 3.10 shows three typical externally measured inertance FRFs taken during an experimental data collection run on the GE A4. These FRFs indicate expected structural behavior in the region from 0 to approximately 50 Hertz. Also clearly shown are the large acceleration magnitudes at 71 and 88 Hertz, caused by the relative flexibility of the vertical link, as described above.

Resulting vibrational parameter estimates for three typical parameters are shown in Figure 3.11. This figure indicates clearly that individual parameters (which represent individual manipulator physical quantities) have different predicted spectral

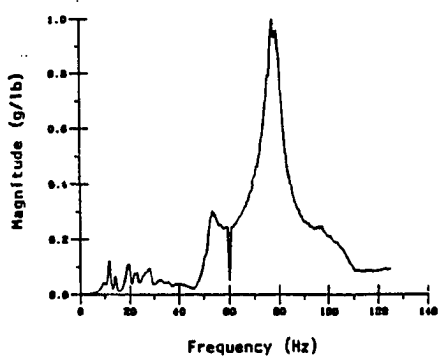Table 3.1: Modal Frequencies, General Electric Model A4 Manipulator

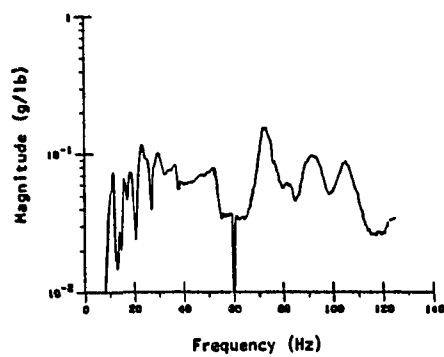| Mode	Frequency
1	9 Hz
2	12
3	15
4	18
5	26
6	31
7	37
8	48
9	52
10	56
11	71
12	88
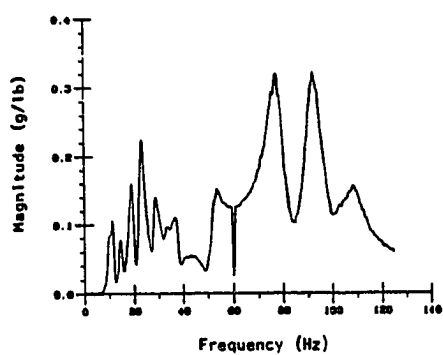
a) Local X-Direction
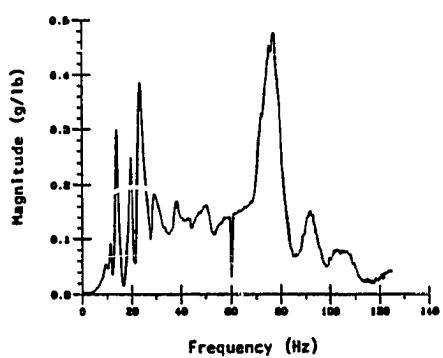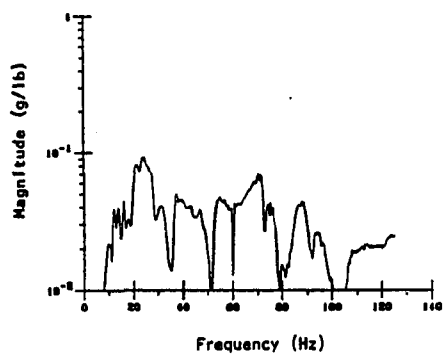

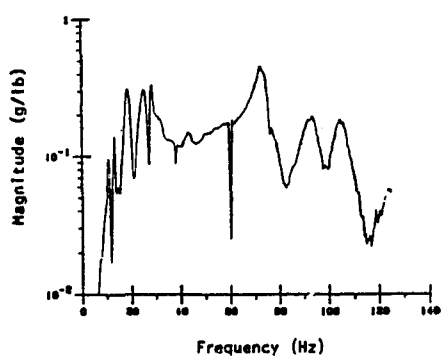b) Local Y-Direction

c) Local Z-Direction

Figure 3.10: Typical Externally Measured Frequency Response Functions, Posture 9, Accelerometer Location 16

a) Parameter 7 (Upper Arm Lateral
   Dimension, a_2)

b) Parameter 8 (Upper Arm Longitudinal
   Dimension, b_2)

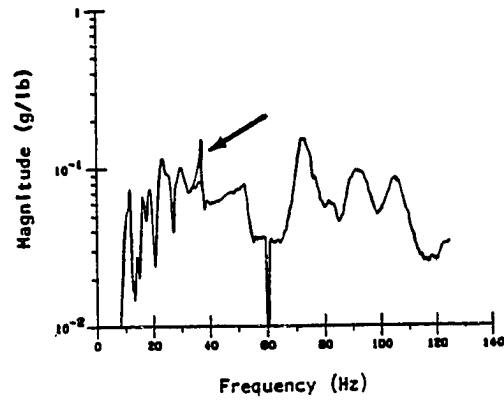c) Parameter 9 (Upper Arm Vertical
   Dimension, c_2)

Figure 3.11: Typical Vibrational Parameter Estimates, Parameters 7, 8, and 9

contributions to vibrations at the end effector. For example, Parameters 7 (upper arm lateral dimension, a_2) and 9 (upper arm vertical dimension, c_2) are predicted to make significant contributions to the 71-Hertz mode, while parameter 8 (upper arm longitudinal dimension, b_2) makes a very small contribution to this mode.

All frequency response functions described in the figures above show a notch at 60 Hertz. This notch is attributable to observed uncorrelated 60-Hertz noise in the system input signal. Also, as in previous FRF plots, data below 3 Hertz must be discounted.

As in the static calibration, the most serious consideration in interpretation of the synthesized vibrational parameter estimates proved to be existence of redundant parameters in the GE A4, and therefore in its mathematical model. These redundant parameters do not preclude a useful mathematical solution, but do present problems in relating values of the synthesized parameters to values of the corresponding manipulator elements.

The following theoretical example demonstrates the potential for use of the vibrational calibration algorithm to supply data for a manipulator predictive maintenance program. If, for instance, one of the radial ball bearings in the base/upper-arm joint begins to fail in the radial direction, increased vibrations would be expected at frequencies characteristic of the failure of this particular ball bearing. Taking Figure 3.11 as an example of the vibrational parameters of a "healthy" manipulator, Figure 3.12 shows the trends in the vibrational parameters which may be expected as the ball bearing fails. Figures 3.12a and 3.12b show increased vibration levels at approximately 36 Hertz in the two horizontal (ball bearing radial) directions, but relatively little increase in the vertical (ball bearing thrust) direction. Further experience with the vibrational calibration procedure applied over the long-term to real manipulators will allow geometric isolation of such failing components.

a) Parameter 7 (Upper Arm Lateral Dimension, a_2)
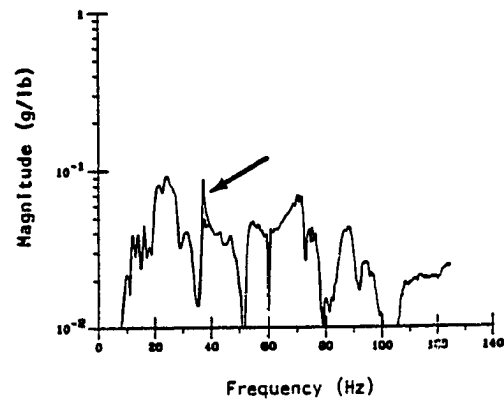
b) Parameter 8 (Upper Arm Longitudinal Dimension, b_2)
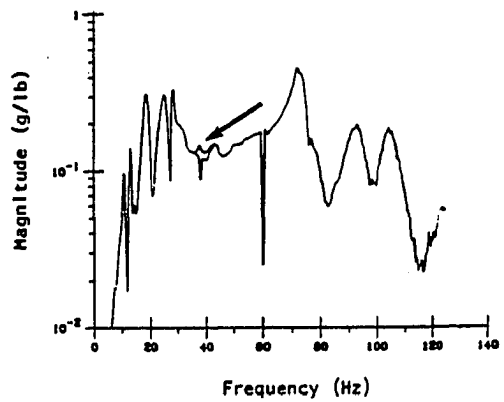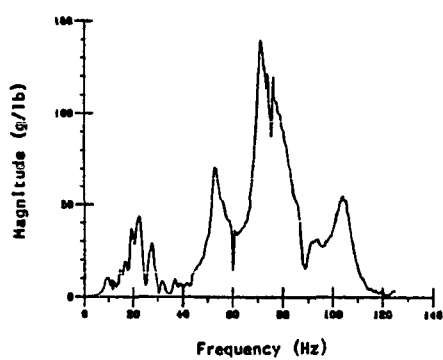
c) Parameter 9 (Upper Arm Vertical Dimension, c_2)

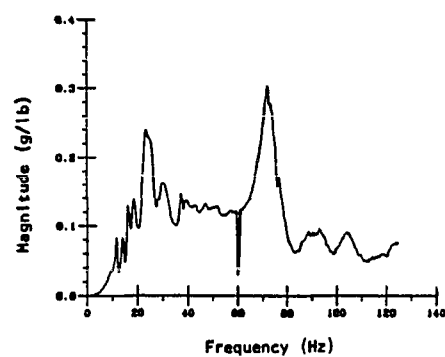Figure 3.12: Theoretical Vibrational Parameter Estimates with Failing Bearing, Parameters 7, 8, and 9

3.4 Conclusions

Comments made in Section 2.4 regarding the identification and handling of redundant parameters also apply for the vibrational calibration scheme. Presence of redundant parameters may cause synthesized parameter values to vary *widely* from the corresponding manipulator element dimensions/values. This is shown in Figure 3.13, which represents the synthesized parameters of a vibrational calibration. In this calibration, the same input (external) vibrational data was used as was used in the calibration which produced the parameters of Figure 3.11. The only difference between the two calibrations was that, in the latter calibration, a parameter describing the zero-reference angle of the waist rotation (parameter 43, θ_{01}) was optimized in addition to the original three. The new parameter is strongly redundant with the parameter which describes the lateral dimension of the upper arm (parameter 7, a_2). This redundancy causes the average magnitude of the upper arm lateral dimension to change by approximately three orders of magnitude between the first calibration and the second. Parameters 8 (upper arm longitudinal dimension, b_2) and 9 (upper arm vertical dimension, c_2) are affected also, but to a much lesser extent. This type of parameter behavior was also observed in static calibrations by Stone, Sanderson, and Neuman [16]. Much additional work is necessary to refine understanding of the relationship between mathematical and physical parameters.

The vibrational calibration offers many of the advantages of a multiple-posture modal analysis but at a substantial savings in data collection and analysis times. In addition, the vibrational calibration scheme allows *quantitative* prediction of the vibrational characteristics of different physical parts of the manipulator. (Alternatively, no viable approach to quantitatively interpreting multiple-posture modal analyses has yet been developed.) The predicted FRFs for these parameters are averaged quantities, resulting from vibrational data measured throughout the manipulator's workspace. Additional experience in applying the vibrational calibration to real manipulators will allow isolation/identification of wearing or failing manipulator

a) Parameter 7 (Upper Arm
Lateral Dimension, a_2)

c) Parameter 9 (Upper Arm
Vertical Dimension, c_2)
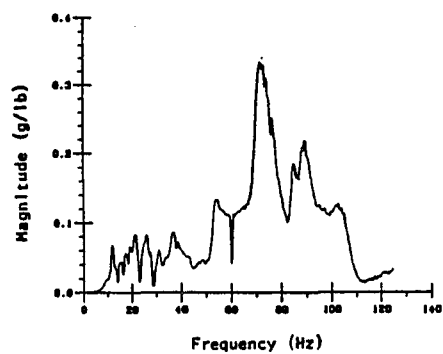
b) Parameter 8 (Upper Arm
Longitudinal Dimension, b_2)

d) Parameter 43 (Waist Rotation
Zero-Reference Angle, θ_{01})

Figure 3.13: Typical Vibrational Parameter Estimates, Redundant Parameter in
Calibration, Parameter 7, 8, 9, and 43

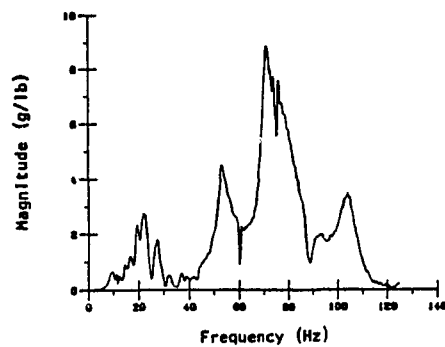components before such isolation could be made economically by other means. The vibrational calibration algorithm performs a *geometric* decomposition of EECF vibrations and cannot, of course, predict modal mass, stiffness, or damping parameters.

Research objectives met in this chapter include:

1. modification and extension of the static calibration algorithm to carry out the vibrational calibration of a robotic manipulator,

2. numerical implementation of the vibrational calibration algorithm, and

3. testing of the vibrational calibration algorithm using data from a real industrial robot.

3.5 Summary

This chapter presents a general, flexible, efficient approach to vibrational kinematic parameter estimation for robotic manipulators. The combination of external vibrational measurement, numerical kinematic synthesis, and manipulator kinematic model correction allows re-evaluation of selected elements in the vibrational parameter set which analytically describes such manipulators. Use of these synthesized parameter spectral estimates permits characterization of composite vibrational properties of manipulator parameters based on vibrational data collected throughout the workspace. Predictive maintenance and repair of manipulators will be important practical application areas for the vibrational calibration procedure.

Chapter 4

SUMMARY

Experimental estimation of the kinematic parameters of robotic manipulators provides a means for increasing the absolute positioning accuracy of the manipulator's end effector without the expense of tighter tolerances on manipulator components. Two approaches to parameter estimation, static and vibrational, are considered in the current work.

The static parameter estimation may be expressed as a multiple-point synthesis of the "optimal" kinematic parameters of a spatial open-loop mechanism for rigid-body guidance. Considerable latitude exists in the choice of the kinematic parameters to be estimated for a particular manipulator; typical choices include parameters describing link geometry, joint transducer zero-offsets, and joint transducer slopes. Accurate measurement of absolute end effector pose (both position and attitude) must be made by external means at several manipulator postures and compared to the corresponding poses predicted by the manipulator's internal kinematic model. Accumulation of differences between these internal pose calculations and external pose measurements at many such postures over the anticipated range of manipulator motion will allow re-evaluation of initial parameter estimates to minimize aggregate error over the estimation space. The external experimental pose measurements must have an absolute accuracy significantly better than the accuracy desired for the synthesized optimal manipulator model. Absolute end effector accuracy is then improved by replacing the nominal parameter values in the manipulator's internal kinematic model with the synthesized optimal parameter values.

The static parameter estimation procedure was tested using data collected from a General Electric model A4 industrial robot for a number of different test conditions. The most important consideration in interpreting the experimental results was the presence (or absence) of redundant parameters in the synthesized model - a problem which may be reduced by including data from estimation sites other than at the manipulator's end effector.

Just as the static parameter estimation predicts the relationship between the various kinematic parameter values and absolute end effector location, the vibrational parameter estimation predicts the relationship between vibrations in the various component parameters and vibrations at the end effector. In the vibrational estimation, an accurate external measurement must be made of forced vibrations of the end effector. Once the vibrational data is available for the end effector at several postures over the anticipated range of manipulator motion, a synthesis procedure similar to that used in the static phase is used at any of several time/frequency combinations, producing time- and frequency-domain descriptions of each of the optimal parameters.

The vibrational parameter estimation procedure was tested on the same General Electric robot as used in the static estimation. Several descriptions were obtained for the behavior of particular parameters in both the time and the frequency domains. In addition, a modal analysis of the A4 was performed at one posture for comparison to both the vibrational parameter estimation data and to other modal analyses of the General Electric A4. Specific issues addressed in the vibrational phase included the effects on manipulator vibrational response of (1) the robot's closed-loop servo-control system, (2) vibrational input power, and (3) orientation of input forcing. Items 1 and 2 above were shown to have very little effect on manipulator vibrational response. Orientation of input forcing, however, was shown to have a potentially significant effect, and further research was recommended to better assess that effect. The vibrational parameter estimation has the important advantage of providing information similar to that provided by modal analysis at multiple postures, while requiring significantly less data collection.

One important application of both the static and vibrational estimations will be in the predictive maintenance of industrial robots, in which the vibrational response of a robot is tracked over an extended period of time for the purpose of determining maintenance requirements. Both parameter estimation techniques have proven to be viable methods in the laboratory, and are being refined for practical industrial use.

Both the static and vibrational calibration research programs have indicated the need for additional research in several areas:

- experimental use of multiple calibration points per calibration posture to reduce the effects of redundant parameters,

- exploration of more practical methods of external pose data collection, vibrational excitation, and vibrational measurement,

- exploration and quantification of the effects of input direction on manipulator vibrational response,

- long-term experience in correlating optimized parameter histories with observed mechanical wear/failure of manipulator components, and

- development and testing of the dynamic level of manipulator calibration, which includes the effects of gross component motion and deflection.

Appendix A

KINEMATIC MODELS
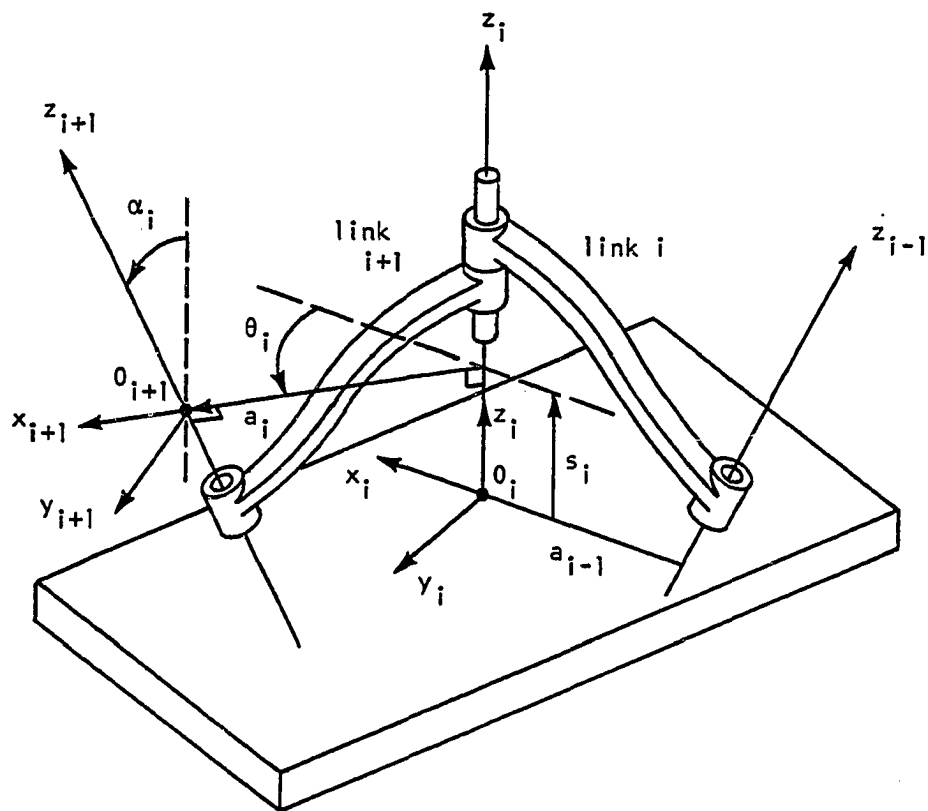
O_i = Origin of Coordinate System i

z_i = Axis of Revolute Connecting Link i and Link i+1

x_i = Axis Formed by Common Perpendicular from z_{i-1} to z_i

y_i = Axis to Complete Right-Hand Coordinate System

a_i = Length of Common Perpendicular from z_i to z_{i+1}

s_i = Distance along z_i from x_i to x_{i+1}

α_i = Angle from z_i to z_{i+1} about x_{i+1}

θ_i = Angle from x_i to x_{i+1} about z_i

Figure A.1: Denavit-Hartenberg Kinematic Notation (after Uicker, Denavit, and Hartenberg [17])
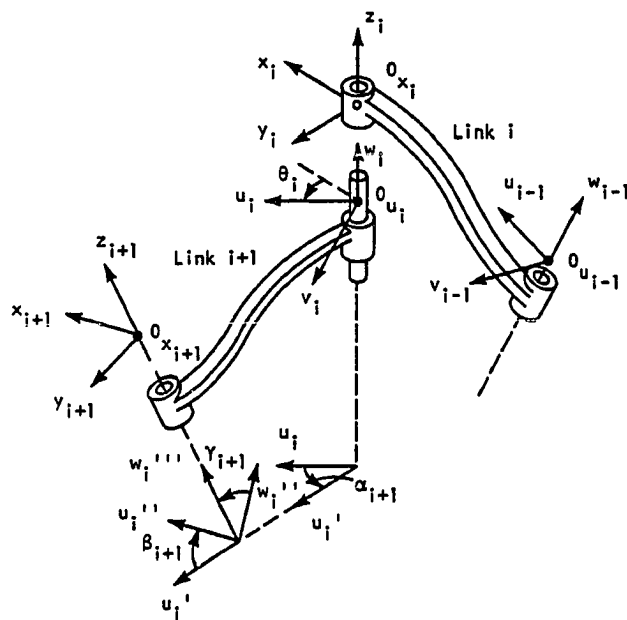
0_{x_i} = Origin of Coordinate System $x_i y_i z_i$ (Coincident with 0_{u_i})

z_i = Axis of Revolute Connecting Link i and Link i+1

x_i = Axis Perpendicular to z_i (Location Arbitrary)

y_i = Axis to Complete Right-Hand Coordinate System

$\quad$ ($x_i y_i z_i$ is fixed in link i)

0_{u_i} = Origin of Coordinate System $u_i v_i w_i$ (Coincident with 0_{x_i})

w_i = Axis of Revolute Connecting Link i and Link i+1

v_i = Axis Perpendicular to w_i

u_i = Axis to Complete Right-Hand Coordinate System

$\quad$ ($u_i v_i w_i$ is fixed in link i+1)

θ_i = Angle from x_i to u_i about z_i (Joint Variable for Joint i)

a_i = u_i-Location of $0_{x_{i+1}}$ within $u_i v_i w_i$ (Not Shown)

b_i = v_i-Location of $0_{x_{i+1}}$ within $u_i v_i w_i$ (Not Shown)

c_i = w_i-Location of $0_{x_{i+1}}$ within $u_i v_i w_i$ (Not Shown)

α_i = Angle from u_i to u_i' about w_i

β_i = Angle from u_i' to u_i'' about v_i'

γ_i = Angle from w_i'' to w_i''' about u_i''

$\quad$ ($u_i''' v_i''' w_i'''$ has the same attitude as $x_{i+1} y_{i+1} z_{i+1}$)

Figure A.2: "Extended" Kinematic Notation (after Sheth and Uicker [18])

Appendix B

CALIBRATION POSTURES

posture	θ_1	θ_2
1	39.2°	-19.6°
2	25.5°	-22.4°
3	9.2°	-26.3°
4	-6.2°	-43.7°
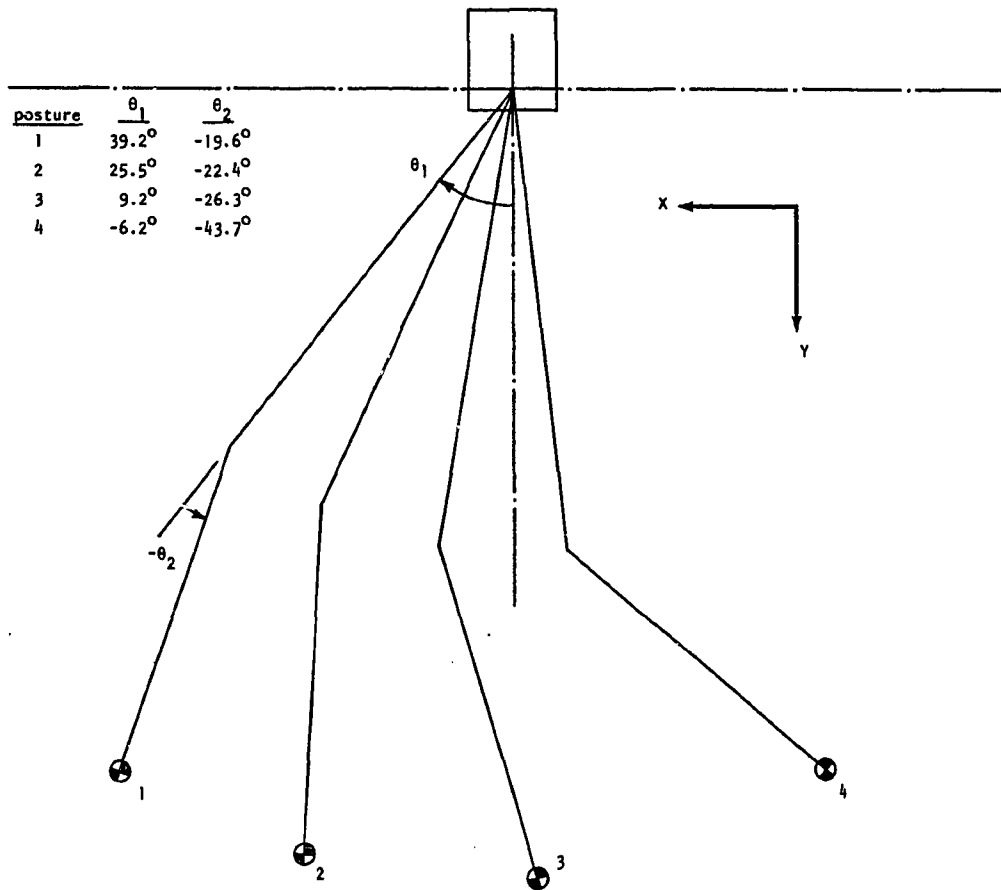
Figure B.1: Schematic of Calibration Postures 1 Through 4, General Electric Model A4 Manipulator (Top View)

posture	θ_1	θ_2
5	-2.6°	-50.3°
6	21.5°	-67.6°
7	24.6°	-34.3°
8	43.0°	-25.6°
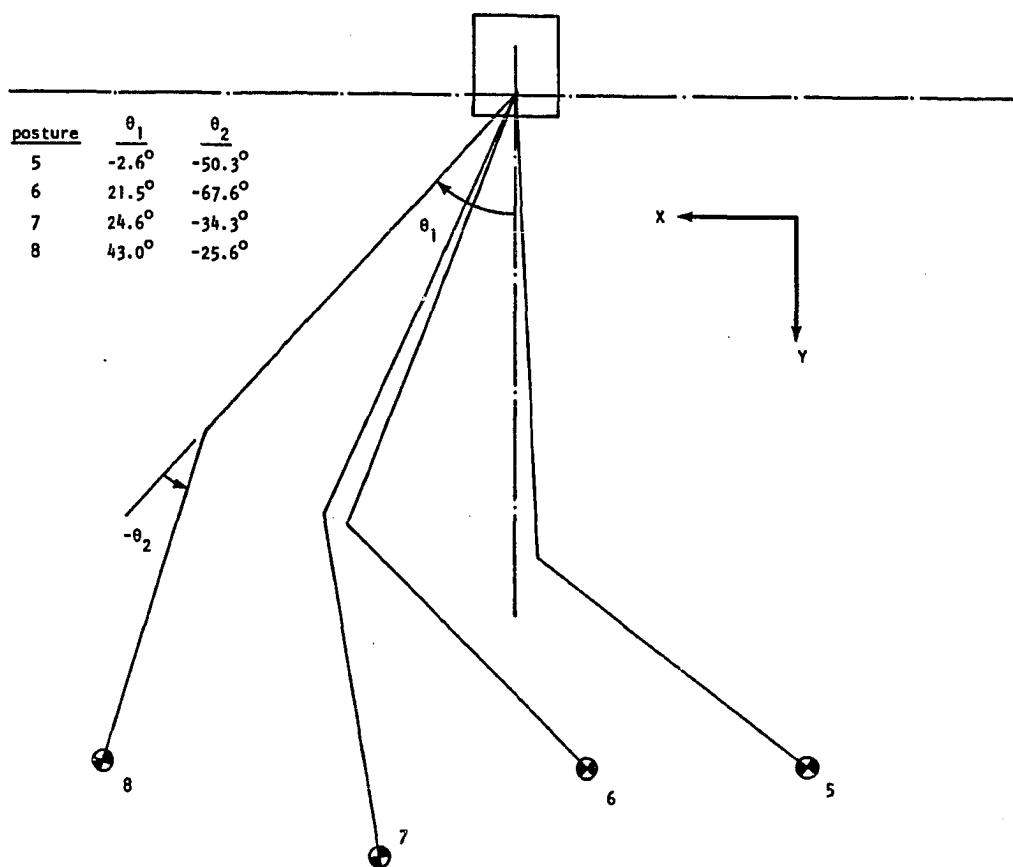
Figure B.2: Schematic of Calibration Postures 5 Through 8, General Electric Model A4 Manipulator (Top View)

posture	θ_1	θ_2
9	45.4°	-28.4°
10	42.6°	-66.1°
11	11.5°	-37.0°
12	-11.0°	-26.6°
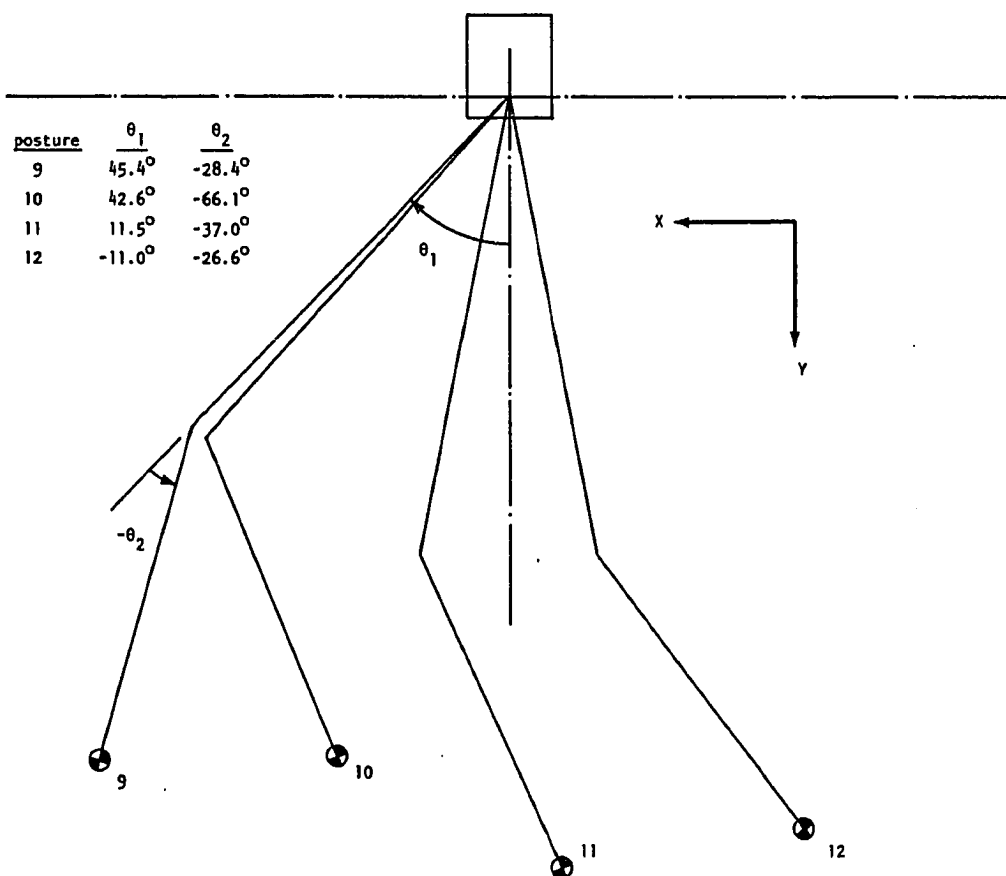
Figure B.3: Schematic of Calibration Postures 9 Through 12, General Electric Model A4 Manipulator (Top View)

posture	θ_1	θ_2
13	2.7°	-80.7°
14	26.8°	-96.4°
15	50.4°	-97.0°
16	66.4°	-69.6°
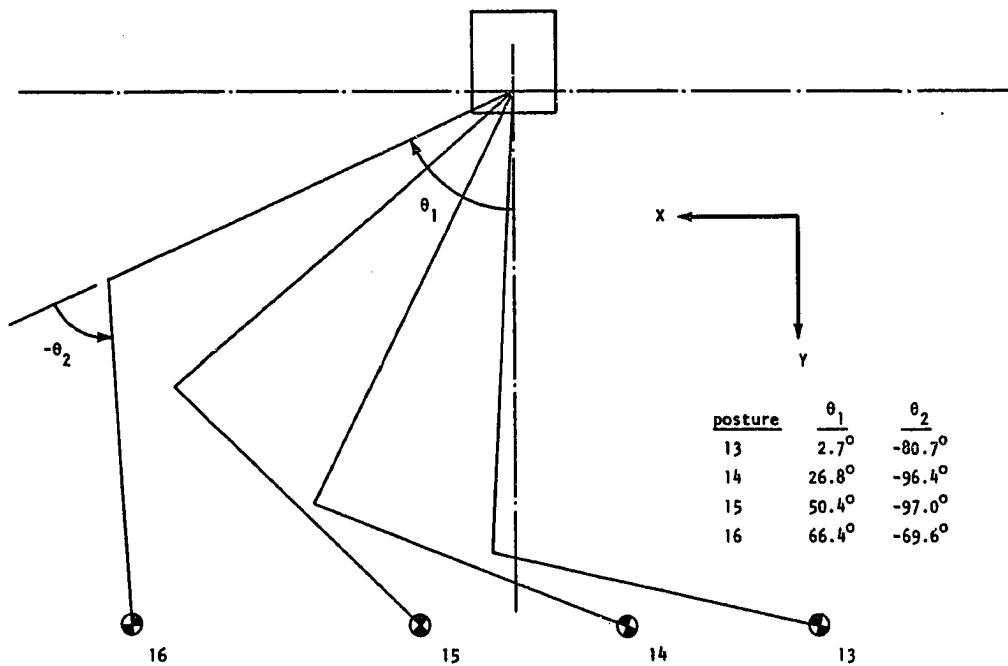
Figure B.4: Schematic of Calibration Postures 13 Through 16, General Electric Model A4 Manipulator (Top View)

posture	θ_1	θ_2
17	68.6°	-74.7°
18	59.1°	-96.0°
19	34.4°	-94.3°
20	4.0°	-86.9°
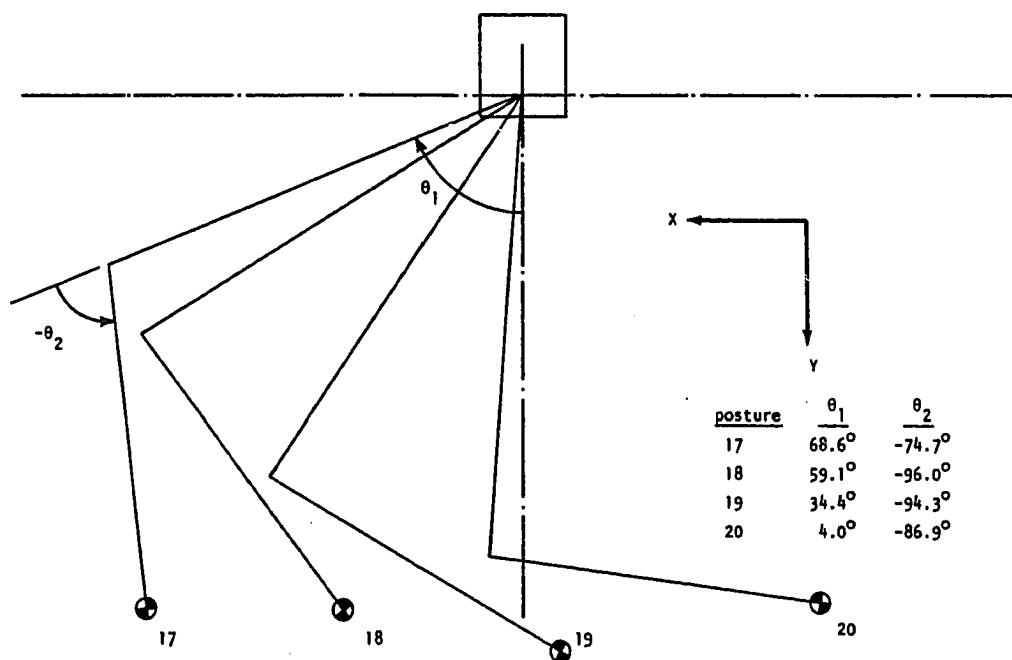
Figure B.5: Schematic of Calibration Postures 17 Through 20, General Electric Model A4 Manipulator (Top View)

posture	θ_1	θ_2
21	5.1°	-85.8°
22	53.9°	-101.4°
23	66.6°	-67.0°
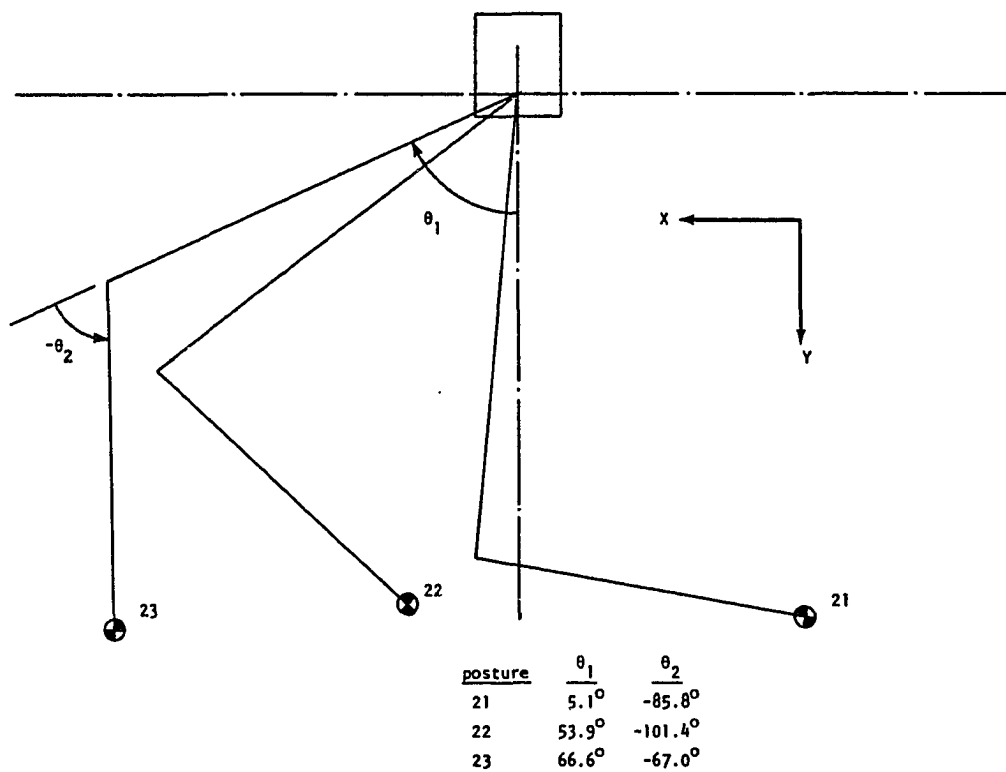
Figure B.6: Schematic of Calibration Postures 21 Through 23, General Electric Model A4 Manipulator (Top View)

posture	θ_1	θ_2
24	91.3°	-97.9°
25	83.1°	-122.3°
26	51.5°	-127.5°
27	21.8°	-125.5°
28	0.1°	-113.8°
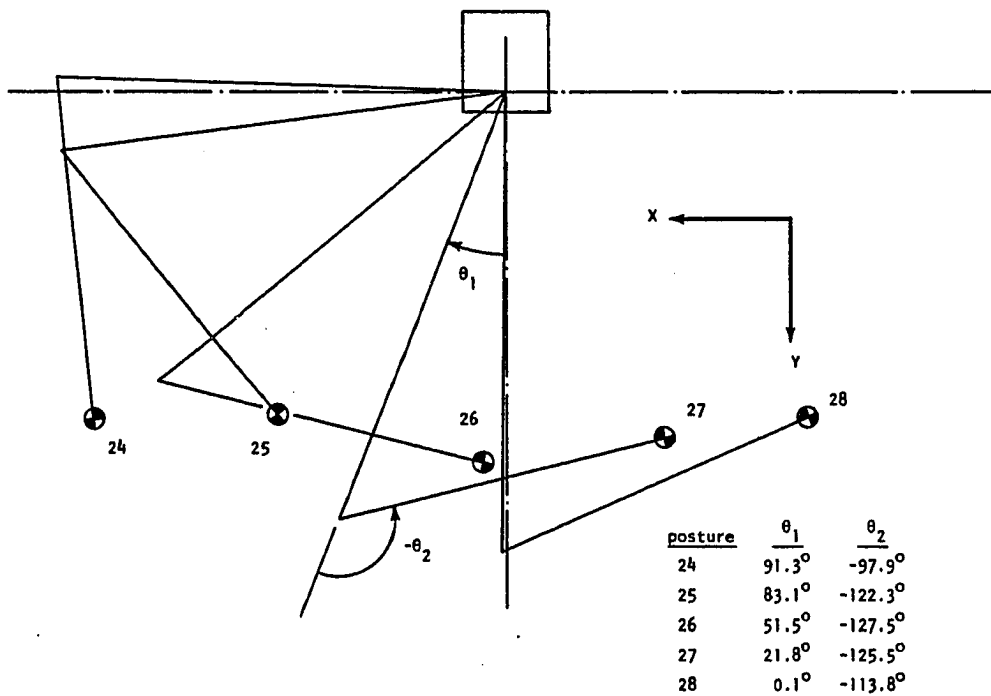
Figure B.7: Schematic of Calibration Postures 24 Through 28, General Electric Model A4 Manipulator (Top View)

posture	θ_1	θ_2
29	3.3°	-113.8°
30	32.6°	-127.6°
31	72.7°	-130.6°
32	89.3°	-100.5°
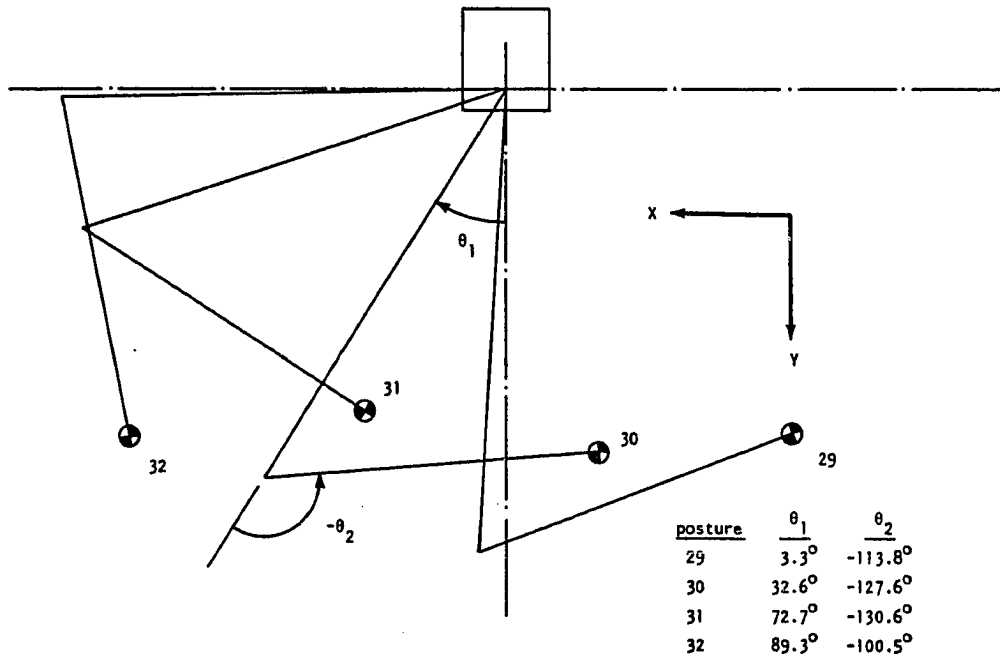
Figure B.8: Schematic of Calibration Postures 29 Through 32, General Electric Model A4 Manipulator (Top View)

posture	θ_1	θ_2
33	88.4°	-101.3°
34	69.9°	-122.4°
35	38.8°	-133.4°
36	-0.9°	-115.1°
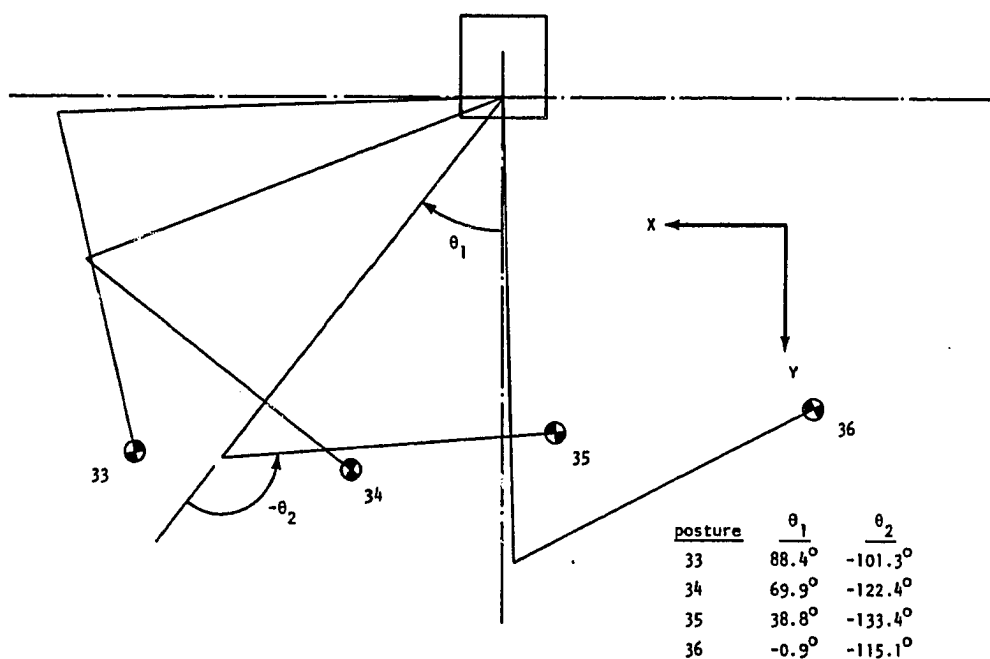
Figure B.9: Schematic of Calibration Postures 33 Through 36, General Electric Model A4 Manipulator (Top View)

Appendix C

TYPICAL $[X]^T[X]$ MATRICES

	a_1	b_1	b_2	c_2	b_3	θ_{01}	θ_{02}	
	35.96	0.000	18.63	0.000	-19.58	640.9	244.5	a_1
	0.000	35.96	25.12	0.000	20.43	-64.21	229.7	b_1
	18.63	25.12	35.95	0.000	4.008	340.7	340.6	b_2
	0.000	0.000	0.000	35.96	0.000	0.000	0.000	c_2
	-19.58	20.43	4.008	0.000	35.98	-458.3	-1.126	b_3
	640.9	-64.21	340.7	0.000	-458.3	15,530	5,795	θ_{01}
	244.5	229.7	340.6	0.000	-1.126	5,795	5,011	θ_{02}

Figure C.1: Typical $[X]^T[X]$ Matrix, Calibration Data Collection Run I, Final (3rd) Iteration, Special Case: 7 Optimized Parameters, None Redundant

	a_1	b_1	b_2	c_2	b_3	c_3	θ_{01}	θ_{02}	
	35.96	0.000	18.63	0.000	-19.58	0.000	640.9	244.5	a_1
	0.000	35.96	25.12	0.000	20.43	0.000	-64.21	229.7	b_1
	18.63	25.12	35.95	0.000	4.008	0.000	340.7	340.6	b_2
	0.000	0.000	0.000	35.96	0.000	35.96	0.000	0.000	c_2
	-19.58	20.43	4.008	0.000	35.98	0.000	-458.3	-1.126	b_3
	0.000	0.000	0.000	35.96	0.000	35.96	0.000	0.000	c_3
	640.9	-64.21	340.7	0.000	-458.3	0.000	15,528	5,795	θ_{01}
	244.5	229.7	340.6	0.000	-1.126	0.000	5,795	5,011	θ_{02}

Figure C.2: Typical $[X]^T[X]$ Matrix, Calibration Data Collection Run I, Final (3rd) Iteration, Special Case: 8 Optimized Parameters, c_2 and c_3 Redundant

REFERENCES

[1] Kinzel, G. L. and Hall, A. S., Jr., "Tolerances and Clearances in Instrumented Spatial Chains," *Fourth World Congress on the Theory of Machines and Mechanisms*, London, Institute of Mechanical Engineers, 1975, pp. 185-191.

[2] Mooring, B. W., "The Effect of Joint Axis Misalignment on Robot Positioning Accuracy," *Computers in Engineering*, ASME, Vol. 2, 1983, pp. 151-155.

[3] Stauffer, R. N., "Robot Accuracy," *Robotics Today*, Vol. 2, No. 7 (April 1985), pp. 43-49.

[4] Colson, J. C. and Perreira, N. D., "Robotic System Pose Performance: Definitions and Analysis," *Computers in Engineering*, ASME, Vol. 1, 1985, pp. 247-257.

[5] Sommer, H. J. III and Miller, N. R., "A Technique for the Calibration of Instrumented Spatial Linkages Used for Biomechanical Kinematic Measurements," *Journal of Biomechanics*, Vol. 14, No. 2 (February 1981), pp. 91-98.

[6] Tull, H. G. III and Lewis, D. W., "Three-Dimensional Kinematic Synthesis," *Journal of Engineering for Industry, Transactions ASME*, Vol. 90, No. 3 (August 1968), pp. 481-484.

[7] Chen, F. Y. and Chan, V.-L., "Dimensional Synthesis of Mechanisms for Function Generation Using Marquardt's Compromise," *Journal of Engineering for Industry, Transactions ASME*, Vol. 96, No. 1 (February 1974), pp. 131-137.

[8] Marquardt, D. W., "An Algorithm for Least-Squares Estimation of Nonlinear Parameters," *Journal of the Society for Industrial and Applied Mathematics*, Vol. 11, No. 2 (June 1963), pp. 431-441.

[9] Scheffer, B., "Geometric Control and Calibration Method of an Industrial Robot," *Twelfth International Symposium on Industrial Robots and Sixth International Conference on Industrial Robot Technology*, Paris, June 9-11, 1982, pp. 331-339.

[10] Spur, G., Duelen, G., and Kirchoff, U., "A Process for the Determination of the Zero Position Values and Lengths of Elements in Kinematic Chains," Paper No. MS84-498, Robotics International of SME, Dearborn, Michigan, 1984.

[11] Mooring, B. W. and Tang, G.-R., "An Improved Method for Identifying the Kinematic Parameters in a Six Axis Robot," *Computers in Engineering*, ASME, Vol. 1, 1984, pp. 79-84.

[12] Whitney, D. E., Lozinski, C. A., and Rourke, J. M., "Industrial Robot Calibration Method and Results," *Computers in Engineering*, ASME, Vol. 1, 1984, pp. 92-100.

[13] Kirchner, H. O. K., Gurumoorthy, B., and Prinz, F. B., "A Perturbation Approach to Robot Calibration," Paper No. CMU-RI-TR-85-9, The Robotics Institute, Carnegie-Mellon University, Pittsburgh, Pennsylvania, April 1985.

[14] Ibarra, R. and Perreira, N. D., "Determination of Linkage Parameter and Pair Variable Errors in Open Chain Kinematic Linkages Using a Minimal Set of Pose Measurement Data," ASME paper no. 85-DET-51, accepted for publication in *Journal of Mechanisms, Transmissions, and Automation in Design, Transactions ASME*.

[15] Hsu, T.-W. and Everett, L. J., "Identification of the Kinematic Parameters of a Robot Manipulator for Positional Accuracy Improvement," *Computers in Engineering*, ASME, Vol. 1, 1985, pp. 263-267.

[16] Stone, H. W., Sanderson, A. C., and Neuman, C. P., "Arm Signature Identification," *Proceedings of the IEEE International Conference on Robotics and Automation*, Vol. 1, Computer Society Press, San Francisco, California, April 7-10, 1986, pp. 41-48.

[17] Uicker, J. J. Jr., Denavit, J., and Hartenberg, R. S., "An Iterative Method for the Displacement Analysis of Spatial Mechanisms," *Journal of Applied Mechanics, Transactions ASME*, Vol. 31, No. 2 (June 1964), pp. 309-314.

[18] Sheth, P. N. and Uicker, J. J., Jr., "A Generalized Symbolic Notation for Mechanisms," *Journal of Engineering for Industry, Transactions ASME*, Vol. 93, No. 1 (February 1971), pp. 102-112.

[19] Koliskor, A. Sh. and Kochenov, M. I., "Methods for Checking the Operating Accuracy of Industrial Robots," *Machines & Tooling*, Vol. 49, No. 8 (1978), pp. 7-10.

[20] Gendron, W. A. and Sommer, H. J. III, "Pulsed Sonic Coordinate Digitization Using Point-Effect Microphones," *Rovotics Research and Advanced Applications*, ASME, 1982, pg. 167.

[21] Lau, K., Hocken, R., and Haight, W., "An Automatic Laser Tracking Interferometer System for Robot Metrology," internal publication, National Bureau of Standards, Gaithersburg, Maryland, March 1985.

[22] Lau, K., Hocken, R., and Haynes, L., "Robot Performance Measurements Using Automatic Laser Tracking Techniques," internal publication, Center for Manufacturing Engineering, National Bureau of Standards, Gaithersburg, Maryland.

[23] Warnecke, H.-J., Brodbeck, B., and Schiele, G., "Comparative Evaluation of Industrial Robot Accuracy," *Precision Engineering*, Vol. 2, No. 2 (April 1980), pp. 89-92.

[24] Ho, C. Y., "Study of Precision and Calibration for IBM RS-1 Robot System," *Assembly Automation*, Vol. 2, No. 4 (November 1982), pp. 198-201.

[25] Mooring, B. W., Bingham, D. N., and Hoffman, J., "Enhancement of Repeatability during Warm-Up for the IBM 7565 Robot," *Computers in Engineering*, ASME, Vol. 1, 1985, pp. 259-262.

[26] Draper, N. R. and Smith, H., *Applied Regression Analysis*, 2nd Edition, New York, John Wiley & Sons, 1981.

[27] Uicker, J. J., Jr., "Dynamic Behavior of Spatial Linkages, Part 2 - Small Oscillations About Equilibrium," *Journal of Engineering for Industry, Transactions ASME*, Vol. 91, No. 1 (February 1969), pp. 258-265.

[28] Broch, J. T., *Mechanical Vibration and Shock Measurements*, Denmark, Brüel & Kjær, 1980.

[29] Halvorsen, W. G. and Brown, D. L., "Impulse Technique for Structural Frequency Response Testing," *Sound and Vibration*, Vol. 11, No. 11 (November 1977), pp. 8-21.

[30] Kirshenboim, J. and Ewins, D. J., "A Method for Recognizing Structural Nonlinearities in Steady-State Harmonic Testing," *Journal of Vibration, Acoustics, Stress, and Reliability in Design, Transactions ASME*, Vol. 106, No. 1 (January 1984), pp. 49-52.

[31] Stoltzfus, T. and Young, D. K., "Modal Analysis of a GE P50 Robot," internal publication, Department of Mechanical Engineering, Pennsylvania State University, University Park, Pennsylvania, May 1984.

[32] Berger, J., Fessler, C., and Kaylor, B., "Three-Dimensional Modal Analysis of a General Electric A-3 Robot," internal publication, Department of Mechanical Engineering, Pennsylvania State University, University Park, Pennsylvania, May 1984.

[33] Ramsey, K. A., "Effective Measurements for Structural Dynamics Testing, Part II," *Sound and Vibration*, Vol. 10, No. 4 (April 1976), pp. 18-31.

[34] Bendat, J. S. and Piersol, A. G., *Engineering Applications of Correlation and Spectral Analysis*, New York, John Wiley & Sons, 1981.

[35] Dagalakis, N. G. and Myers, D. R., "Adjustment of Robot Joint Gear Backlash Using the Robot Joint Test Excitation Technique," *The International Journal of Robotics Research*, Vol. 4, No. 2 (Summer 1985), pp. 65-79.

VITA

James R. Bosnik, Jr., was born on June 11, 1957, in Saint Marys, Pennsylvania. After graduating from Cameron County High School in Emporium, Pennsylvania, he attended The Pennsylvania State University at the University Park campus, earning B.S. with High Distinction (1981), M.S. (1982), and Ph. D. degrees in Mechanical Engineering. As an undergraduate, he was accepted for membership in Pi Tau Sigma, National Honorary Mechanical Engineering Fraternity, and was certified as a Pennsylvania Engineer-in-Training.

As a master's student, Mr. Bosnik's duties included research into the performance of high-speed elastic linkages, computer systems support, and applications programming. His publications during this time included topics in linkage synthesis and in dynamics of high-speed mechanisms. He was accepted for membership in Sigma Xi, The Scientific Research Society, and was a first-place winner in the Graduate Student Mechanism Design Competition held in conjunction with the 17th Biennial ASME Mechanisms Conference.

In addition to Mr. Bosnik's doctoral research into the static and vibrational calibration of robotic manipulators, he has taught Machine Dynamics, Design of Machine Components, Mechanical Engineering Intrumentation, and Engineering Design, and also has continued with duties in computer systems support and applications programming. During the 1983-84 academic year, he was the recipient of the W. S. Elliott Fellowship (given by the Penn State College of Engineering), and served as the graduate student representative to the College of Engineering Academic Committee.